Pool Boiling on Structured Surfaces: Heat Transfer and Critical Heat Flux

Experiments and Mechanistic Modelling

Cao, Zhen

2019

Document Version:
Publisher's PDF, also known as Version of record

Pool Boiling on Structured Surfaces: Heat Transfer and Critical Heat Flux

-Experiments and Mechanistic Modelling

Zhen Cao

LUNDS UNIVERSITET
Lunds Tekniska Högskola

DOCTORAL DISSERTATION

With permission of the Faculty of Engineering (LTH), Lund University, Sweden. To be defended on Friday 25 October 2019, at 10:15 AM in Lecture Hall M: B in the M-building, Ole Römers väg 1, Lund, Sweden.

Faculty opponent

Professor Jungho Kim

Department of Mechanical Engineering,

University of Maryland, College Park, the United States

Organization LUND UNIVERSITY	Document name DOCTORAL DISSERTATION
Department of Energy Sciences	Date of issue October 25, 2019
Author(s) Zhen Cao	Sponsoring organization China Scholarship Council, Swedish Research Council

Title and subtitle

Pool Boiling on Structured Surfaces: Heat Tranfer and Critical Heat Flux - Experiments and Mechanistic Modelling

Abstract

In this thesis, pool boiling heat transfer was experimentally studied on structured surfaces with dielectric liquids (HFE-7200, NOVEC-649, FC-72), organic liquids (Acetone, Pentane) and deionized water.

In the first step, nanoparticle coatings on copper surfaces were prepared by an electrophoretic deposition method, with Cu-Zn nanoparticles (100 nm) and Cu nanoparticles (150 nm). Two types of nanoparticle-coating surfaces were prepared, namely nanoparticle coatings uniformly deposited on smooth surfaces and nanoparticle coatings partially deposited on smoothsurfaces. Pool boiling of HFE-7200 and acetone was tested on the coating surfaces. It is found that pool boiling heat transfer coefficients are significantly enhanced by nanoparticle coatings. However, the uniform coating cannot enhance the critical heat flux, while the partially-deposited coating can enhance critical heat flux. Mechanistic heat transfer models were developed to predict the heat transfer coefficients, considering natural convection, transient heat conduction, microlayer evaporation and micro convection, while the critical heat flux was analyzed from the point of wickability and hydrodynamic instability.

In the following step, microporous coatings on copper surfaces were generated by an electrochemical deposition method, with electrolyte solutions ($CuSO_4$+H_2SO_4). Pool boiling of HFE-7200, NOVEC-649 and water was tested. The results show that heat transfer coefficients and critical heat flux are enhanced, and the heat transfer coefficients are obviously dependent on deposition-relevant parameters, like deposition time and electrolyte concentration. Heat transfer coefficients were discussed mechanistically and empirically by a mechanistic model and correlations, while the critical heat flux was predicted by a modified force balance model which considers the forces exerted on vapor and assumes occurrence of the critical heat flux when the vapor expands on surfaces.

Finally, hybrid micro/nano structures were fabricated on copper surfaces by femtosecond laser machining and electrophoretic deposition, and on silicon wafers by dry etching and electrostatic deposition. Pool boiling of acetone and FC-72 was investigated on the copper surfaces and the silicon wafers, respectively. It is found that the hybrid structures induce higher heat transfer coefficients than sole structures and wickability plays an important role on enhancement of the critical heat flux.

Key words:

pool boiling, heat transfer, critical heat flux, bubble dynamics, surface modification

Classification system and/or index terms (if any)

Supplementary bibliographical information	Language English
ISSN and key title ISSN 0282-1990 ISRN LUTMDN/TMHP-19/1152-SE	ISBN 978-91-7895-231-1 (print) 978-91-7895-232-8 (pdf)

Recipient's notes	Number of pages 63	Price
	Security classification	

Pool Boiling on Structured Surfaces: Heat Transfer and Critical Heat Flux

-Experiments and Mechanistic Modelling

Zhen Cao

LUNDS UNIVERSITET
Lunds Tekniska Högskola

Department of Energy Sciences

Faculty of Engineering (LTH)

Lund University, Lund, Sweden

www.energy.lth.se

Thesis for the degree of Doctor of Philosophy in Engineering.

Division of Heat Transfer
Department of Energy Sciences
Faculty of Engineering (LTH)
Lund University
Box 118
SE-221 00 LUND
SWEDEN

978-91-7895-231-1 (print)
978-91-7895-232-8 (pdf)
ISRN: LUTMDN/TMHP-19/1152-SE
ISSN: 0282-1990

Printed in Sweden by Media-Tryck, Lund University
Lund 2019

Popular Science

Boiling is the phase change from liquid form to gas form, which occurs when a liquid reaches its boiling point. Bubble nucleation is the physical process associated with boiling. Generally, the nucleation is subdivided into two categories: homogeneous nucleation and heterogeneous nucleation, depending on whether preferential nucleation sites are required or not. The homogeneous nucleation refers to the appearance of a bubble in a superheated liquid pool and far away from bounding walls, while the heterogeneous nucleation is a process in which bubbles form at cavities, scratches and other imperfections on a heated surface submerged in a liquid. Therefore, the heterogeneous nucleation can be enhanced by surface modifications, improving the boiling performance, which is the targeted topic in the present thesis.

Specifically, boiling can be classified as pool boiling and flow boiling. Pool boiling is the boiling in a stagnant liquid, while flow boiling is the boiling in a flowing liquid. Pool boiling heat transfer involves three regimes generally, i.e., nucleate boiling, transitional boiling and film boiling. The nucleate boiling is preferred in practical applications, e.g., microelectronics cooling due to its high heat transfer coefficient (HTC) with small wall superheats, while the critical heat flux (CHF) is a value above which nucleate boiling steps into transitional boiling or even film boiling, deteriorating heat transfer considerably. Accordingly, it is of great significance to augment heat transfer and critical heat flux, and to explore relevant mechanisms. Boiling heat transfer has been investigated for several decades and there is a consensus that boiling performance depends on liquid properties and surface characteristics, although a clear understanding is still lacking. Up to date, numerous technologies have been attempted to modify surfaces, e.g., dry etching, sintering, laser machining and coating. The modification is supposed to change the surface morphology which affects bubble nucleation and bubble dynamics, enhancing boiling performance.

In this thesis, structured surfaces were prepared by several methods, including an electrostatic deposition method, an electrophoretic deposition method, an electrochemical deposition method and femtosecond laser machining. Pool boiling was experimentally studied on structured surfaces with different liquids, i.e., dielectric liquids, organics liquids and water. Accordingly, heat transfer was analyzed mechanistically and empirically, while triggering mechanisms of critical heat flux were explored from the perspective of hydrodynamic instability, wickability and vapor expansion on surfaces. The present work contributed to deepen the understanding of the pool boiling heat transfer significantly. The improved heat transfer coefficient means that the amount of energy for boiling can be reduced. The long term application is intended for heat exchangers.

Abstract

In this thesis, pool boiling heat transfer was experimentally studied on structured surfaces with dielectric liquids (HFE-7200, NOVEC-649, FC-72), organic liquids (Acetone, Pentane) and deionized water.

In the first step, nanoparticle coatings on copper surfaces were prepared by an electrophoretic deposition method, with Cu-Zn nanoparticles (100 nm) and Cu nanoparticles (150 nm). Two types of nanoparticle-coating surfaces were prepared, namely nanoparticle coatings uniformly deposited on smooth surfaces and nanoparticle coatings partially deposited on smoothsurfaces. Pool boiling of HFE-7200 and acetone was tested on the coating surfaces. It is found that pool boiling heat transfer coefficients are significantly enhanced by nanoparticle coatings. However, the uniform coating cannot enhance the critical heat flux, while the partially-deposited coating can enhance critical heat flux. Mechanistic heat transfer models were developed to predict the heat transfer coefficients, considering natural convection, transient heat conduction, microlayer evaporation and micro convection, while the critical heat flux was analyzed from the point of wickability and hydrodynamic instability.

In the following step, microporous coatings on copper surfaces were generated by an electrochemical deposition method, with electrolyte solutions ($CuSO_4$+H_2SO_4). Pool boiling of HFE-7200, NOVEC-649 and water was tested. The results show that heat transfer coefficients and critical heat flux are enhanced, and the heat transfer coefficients are obviously dependent on deposition-relevant parameters, like deposition time and electrolyte concentration. Heat transfer coefficients were discussed mechanistically and empirically by a mechanistic model and correlations, while the critical heat flux was predicted by a modified force balance model which considers the forces exerted on vapor and assumes occurrence of the critical heat flux when the vapor expands on surfaces.

Finally, hybrid micro/nano structures were fabricated on copper surfaces by femtosecond laser machining and electrophoretic deposition, and on silicon wafers by dry etching and electrostatic deposition. Pool boiling of acetone and FC-72 was investigated on the copper surfaces and the silicon wafers, respectively. It is found that the hybrid structures induce higher heat transfer coefficients than sole structures and wickability plays an important role on enhancement of the critical heat flux.

Keywords: pool boiling, heat transfer, critical heat flux, bubble dynamics, surface modification

Acknowledgments

First and foremost, to Professor Bengt Sundén and Associate Professor Zan Wu, my two supervisors, thank you very much for guiding me through my PhD journey step by step. Professor Bengt Sundén, I would like to thank you so much for all conditions that you provided for my PhD study. I enjoyed the relaxing surrounding in our group. Associate Professor Zan Wu, thank you so much for your care and help. You always encouraged and praised me, which inspired me very much. Your work attitude, wisdom and breadth of mind are worth learning for me forever.

Importantly, I would like to thank my colleague, Dr. Sahar Abbood, and the collaborators, Professor Jin-jia Wei, Associate Professor Yong-hai Zhang and Bin Liu from Xi'an Jiaotong University, Xi'an, China. Professor Knut Deppert, Associate Professor Maria Messing and Calle Preger from Nanolund, and Anh-Duc Pham, Dr. Cathrine Albèr and Professor Tautgirdas Ruzgas from Malmö University. Without your help, this thesis could not be what it is.

The former technicians at the department, Martin Carlsson, Mats Bengtsson and Tommy Peterssen deserve many thanks. Especially, Martin Carlsson, thank you so much, helping me with all experimental stuff throughout the whole period. Dr. Peter Falkman, from Malmö University, deserves special and big thanks for the great help with SEM images. I also want to thank NanoLund, a platform that makes many surface characteristic measurements possible.

The administrative staff, Catarina Lindén and Isabelle Frej, and the lab head, Dr. Marcus Lundgren, thank all of you for the kind help with student registration, expense reimbursement, and the coordination of technician's schedule. Without your help, my study in the department would not be so smooth.

For financial support, I first thank the China Scholarship Council that provided me the PhD study scholarship for my living and accommodation in Sweden. The Swedish Research Council (VR) and the Swedish Foundation for International Cooperation in Research and High Education (STINT) are acknowledged for funding the work and visiting studies. I also want to thank the Royal Physiographic Society in Lund and the ÅForsk for supporting me to attend conferences.

Last but not least, I would like to express my special thanks to my family members, my father 曹殿强, my mother 鲁守梅, my aunt 曹佃雪 and my uncle 刘玉良. I really appreciate that you care about me so much. Please set your mind at rest that I already have grown up and I can take care of myself well. Your happiness and health are the best wishes of mine. Finally, Can Meng, my girlfriend, thank you for walking into my life and thank you for the care and love. Let us work hard together to make our tomorrow better.

List of Publications

Publications included in the thesis:

i. **Zhen Cao**, Zan Wu, AnhDuc Pham, Yanjie Yang, Sahar Abbood, Peter Falkman, Tautgirdas Ruzgas, Cathrine Albèr, Bengt Sundén, "Pool boiling of HFE-7200 on nanoparticle-coating surfaces: Experiments and heat transfer analysis", *International Journal of Heat and Mass Transfer*, 2019, Vol. 133, pp. 548-560.

ii. **Zhen Cao**, Zan Wu, Anh-Duc Pham, Bent Sundén, "Electrophoretic deposition surfaces to enhance HFE-7200 pool boiling heat transfer and critical heat flux", *International Journal of Thermal Sciences*, 2019, Vol. 146, pp. 106107.

iii. Zan Wu, **Zhen Cao**, Bengt Sundén, "Saturated pool boiling heat transfer of acetone and HFE-7200 on modified surfaces by electrophoretic and electrochemical deposition", *Applied Energy*, 2019, Vol. 249, pp. 286-299.

iv. **Zhen Cao**, Zan Wu, Bengt Sundén, "Heat transfer prediction and critical heat flux mechanism for pool boiling of NOVEC-649 on microporous copper surfaces", *International Journal of Heat and Mass Transfer*, 2019, Vol. 141, pp. 818-834.

v. **Zhen Cao**, Zan Wu, Bengt Sundén, "Pool boiling of water on coating surfaces: bubble dynamics, heat transfer and critical heat flux", submitted for Journal publication (under review).

vi. Bin Liu, **Zhen Cao**, Yonghai Zhang, Zan Wu, AnhDuc Pham, Wenjun Wang, Zhaoxuan Yan, Jinjia Wei, Bengt Sundén, "Pool boiling heat transfer of N-pentane on micro/nanostructured surfaces", *International Journal of Thermal Sciences*, 2018, Vol. 130, pp. 386-394.

vii. **Zhen Cao**, Bin Liu, Calle Preger, Zan Wu, Yonghai Zhang, Xueli Wang, Maria E. Messing, Knut Deppert, Jinjia Wei, Bengt Sundén, "Pool boiling heat transfer of FC-72 on pin-fin silicon surfaces with nanoparticle deposition", *International Journal of Heat and Mass Transfer*, 2018, Vol. 126, pp. 1019-1033.

Publications not included in the thesis:

i. **Zhen Cao**, Zan Wu, Sahar Abbood, Bengt Sundén, "An analysis of pool boiling heat transfer on nanoparticle-coated surfaces", *Energy Procedia*, 2019, Vol. 158, pp. 5880-5887.

ii. **Zhen Cao**, Calle Preger, Zan Wu, Sahar Abbood, Maria E. Messing, Knut Deppert, Bengt Sundén, "Pool boiling heat transfer of water on copper surfaces with nanoparticles coating", *International Journal of Transport Phenomena*, 2018, accepted for publication.

iii. **Zhen Cao**, AnhDuc Pham, Zan Wu, Tautgirdas Ruzgas, Cathrine Albèr, Bengt Sundén, "Pool boiling heat transfer enhancement of water by gold nanoparticles with an electrophoretic deposition method", *ASME International Mechanical Engineering Congress and Exposition*, November 9-15, 2018, Pittsburgh, Pennsylvania, USA, Paper No. IMECE2018-87356.

iv. **Zhen Cao**, Zan Wu, Bengt Sundén, "Dimensionless analysis on liquid-liquid flow patterns and scaling law on slug hydrodynamics in cross-junction microchannels", *Chemical Engineering Journal*, 2018, Vol. 344, pp. 604-615.

v. **Zhen Cao**, Zan Wu, Jin-yuan Qian, Bengt Sundén, "Water-oil flow in square microchannels with a crossed junction", *ASME 5th Joint US-European Fluids Engineering Division Summer Meeting*, July 15-20, 2018, Montreal, Quebec, Canada, Paper No. FEDSM2018-83056.

vi. **Zhen Cao**, Zan Wu, Mehdi Sattari Najafabadi, Bengt Sundén, "Liquid-liquid flow patterns in microchannels", *ASME 2017 Heat Transfer Summer Conference*, July 9-12, 2017, Bellevue, Washington, USA, Paper No. HT2017-4729.

vii. **Zhen Cao**, Zan Wu, Huibao Luan, Bengt Sundén, "Numerical study on heat transfer enhancement for laminar flow in a tube with mesh conical frustum inserts", *Numerical Heat Transfer, Part A: Application*, 2017, Vol. 72, pp. 21-39.

viii. Zan Wu, **Zhen Cao**, Bengt Sundén, "Flow patterns and slug scaling of liquid-liquid flow in square microchannels", *International Journal of Multiphase Flow*, 2018, Vol 112, pp. 27-39.

ix. Zan Wu, **Zhen Cao**, Bengt Sundén, "Liquid-liquid flow patterns and slug hydrodynamics in square microchannels of cross-shaped junctions", *Chemical Engineering Science*, 2017, Vol 174, pp. 56-66.

Nomenclature

A	heater surface area (m^2)
A_{mct}	cross-section area of a micro-capillary tube (m^2)
A_w	wetting area (m^2)
C_{pl}	specific heat of liquid (J/kg·K)
D_d	bubble departure diameter (m)
D_i	diameter of bubble influenced area, (m) $D_i = D_d$
E	availability, (J)
f	bubble departure frequency (s^{-1})
g	acceleration of gravity (m/s^2)
G	Gibbs free energy (J)
h	liquid drop height in a micro-capillary tube (m)
i_{lv}	latent heat (J/kg)
k_{cu}	thermal conductivity of copper (W/m·K)
k_l	thermal conductivity of liquid (W/m·K)
Na	active nucleation site density (sites/m^2)
P_l	liquid pressure (Pa)
P_v	vapor pressure (Pa)
Pr_l	Prandtl number of liquid
q	heat flux (W/m^2)
q_{cond}	heat flux from transient conduction (W/m^2)
q_{mc}	heat flux from transient micro convection (W/m^2)
q_{me}	heat flux from microlayer evaporation (W/m^2)
q_{nc}	heat flux from natural convection (W/m^2)
r	roughness factor
R	radii of bubbles, (m) or gas constant
R_c	radii of nucleation cavities, (m)
Ra	arithmetic average of the roughness profile, (m)
t	time, (s)
T_b	bubble temperature (K)
T_l	liquid temperature (K)
T_s or T_{sat}	saturated temperature (K)
T_w	boiling surface temperature (K)
T_∞	bulk temperature (K)

Greek symbols

α_l	liquid thermal diffusivity, (m^2/s)
β	thermal expansion coefficient (K^{-1})
δ	thickness of thermal layer, (m)

θ	static contact angle, (°)
θ_{rec}	receding contact angle, (°)
μ_l	liquid dynamic viscosity (Pa·s)
ν_l	liquid kinematic viscosity (m^2/s)
ρ_l	liquid density (kg/m^3)
ρ_v	vapor density (kg/m^3)
σ_{lv}	liquid-vapor surface tension (N/m)

Abbreviations

CHF	critical heat flux, (W/m^2)
CS	composited surface
ECD	electrochemical deposition
EPD	electrophoretic deposition
ESD	electrostatic deposition
FLS	femtosecond laser
HTC	heat transfer coefficient ($W/m^2 \cdot K$)
MEPD	modulated electrophoretic deposition

Table of Contents

1. Introduction 1
   1.1 Background 1
   1.2 Objectives and methodologies 5
   1.3 Outline of the thesis 6
2. State-of-the-Art Literature Review 7
   2.1 Bubble nucleation theory 7
   2.2 Heat transfer mechanism 10
   2.3 Critical heat flux mechanism 12
   2.4 Enhanced boiling surfaces 15
3. Surface Preparation and Test Rigs 19
   3.1 Surface preparation 19
   3.2 Test rigs 25
   3.3 Experimental procedure 28
   3.4 Data reduction and uncertainty analysis 28
4. Results and Discussion 31
   4.1 Validation of the test rig 34
   4.2 Boiling curves 34
   4.3 Bubble dynamics 39
   4.4 Analysis of heat transfer 43
   4.5 Analysis of critical heat flux 47
5. Conclusions and Outlook 53
   5.1 Conclusions 53
   5.2 Outlook 54

Summary of Papers 55

References 58

CHAPTER 1

Introduction

Boiling, a phenomenon that not only relates to people's daily activities in kitchens, but also widely exists in industrial activities, realizing demands of surface cooling and energy conversion. Insights into this topic are important and necessary, which can suggest possible directions to improve the efficiency of the relevant activities. Therefore, studies on boiling are of great significance.

1.1 Background

Electronics cooling

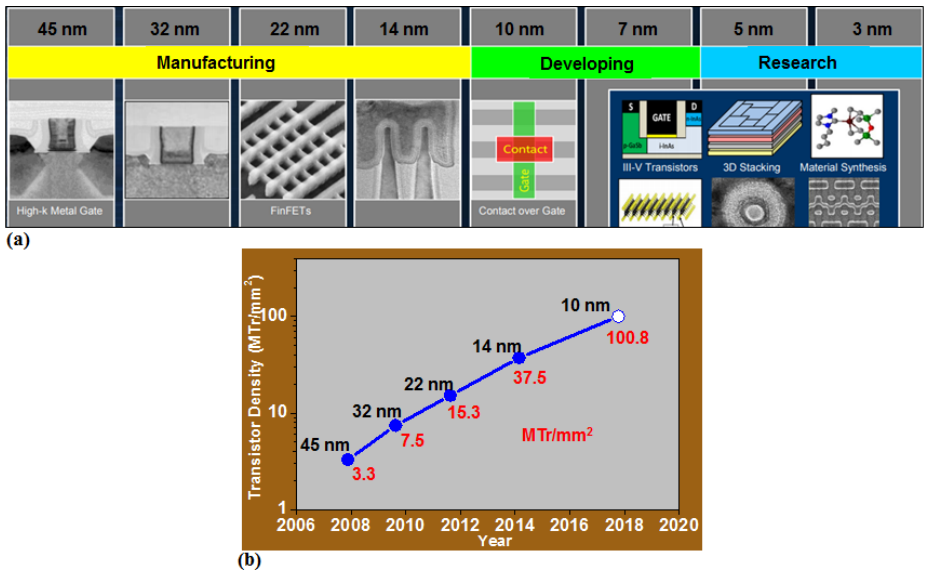

Figure 1.1: Innovation enabled technology pipeline from Intel [1].

The present society is an intelligent society, which closely depends on electronic devices, e.g., computers. In the past decades, with the development of semiconductors, especially progresses on micro/nano manufacturing technologies, miniaturization and integration of electronics become prevailing. For example, as shown in Fig. 1.1(a) about the transistor roadmap in the Intel corporate, transistors become more and more miniaturized. On one hand, the miniaturization brings a large transistor density (Fig. 1.1(b)), which can make electronics perform effectively within a limited space, while on the other hand, dense transistors result in thermal issues. In fact, the lifetime of electronics is dependent on heat generation which occupies around 54% of all electronic failures. As a consequence, a reasonable thermal design of electronic devices is very crucial.

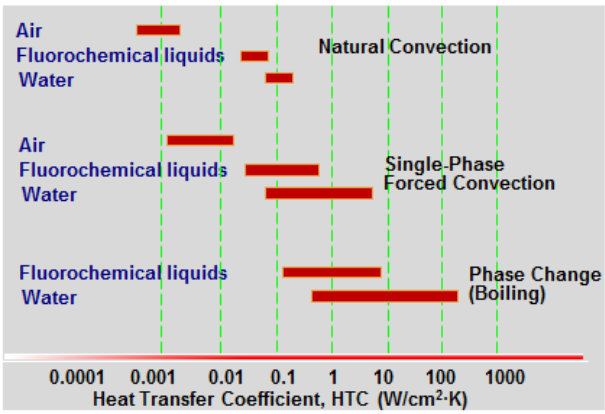

Figure 1.2: Comparison of heat transfer modes [2].

Figure 1.2 compares efficiencies of heat transfer modes, i.e., natural convection, single-phase forced convection and phase change (boiling). Evidently, heat can be dissipated most efficiently with a phase change heat transfer mode. It has been reported that by 2020, the heat load of an individual processor will probably reach up to 140 - 190 W and 210 - 300 W in general servers and in high-performance servers, respectively, while the heat load of servers can reach 1.2-3.3 kW and 7.5-10.5 kW in rackmount servers and in blade servers, respectively [3]. Regarding personal computers or computers for office purposes, a thermal design with air forced convection works to dissipate heat. However, considering super computers or computers for industrial purposes which have much higher power than personal computers, the air forced convection probably does not work anymore. In this case, a more advanced and efficient heat transfer mode is required.

Figure 1.3 illustrates cooling units in commerce, including the widely used air cooling, and recent advanced water cooling and immersion cooling. As is seen, cooling units with phase change heat transfer have been used in real applications, instead of just a conceptual design. Therefore, more studies are needed to optimize the cooling units.

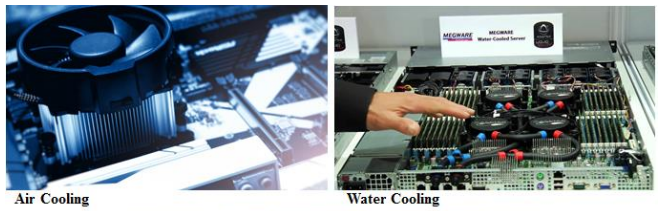

Immersion Cooling (Boiling)

Figure 1.3: Examples of cooling units in applications (from google image and YouTube).

Power generation

Boiling works not only for cooling, but also for energy conversion in power plants. As reported in MIT news [4], around 85% of the worldwide electricity depends on steam power generators. Figure 1.4 describes a basic schematic of a coal power plant where water steam is produced in a boiler by boiling. There are many ways to improve power plant efficiency, like improving coal combustion efficiency and designing advanced thermodynamic cycles, but these are not the present topic. Intuitively, the power plant efficiency can be raised by enhancing the process of steam generation in boilers.

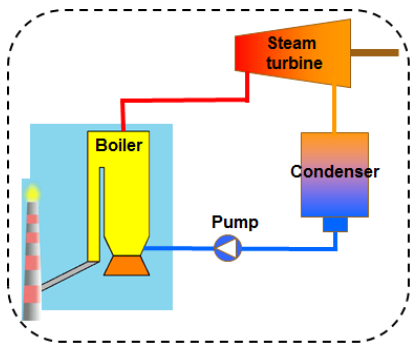

Figure 1.4: Schematic of a coal power plant.

In recent 10 years, energy and environment have become global issues, and power generation technologies have experienced great revolutions, like Organic Rankine Cycle (ORC) to recover waste heat, and solar energy utilization to generate power, as shown in Fig. 1.5. Phase change (boiling) is also a dominant process in these cases, which affects the system efficiency. In an Organic Rankine Cycle, a working fluid is pumped to an evaporator where it boils, passed through an expansion device, and then through a condenser heat exchanger where it

condenses, while in a solar power plant, solar energy converts into thermal energy in a receiver where a working liquid boils.

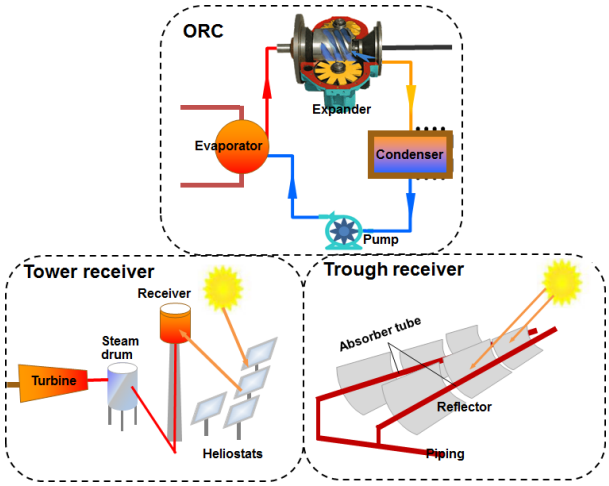

Figure 1.5: Schematics of ORC and solar power plants.

As seen above, boiling is an important physical process in power generation industries. Details of what happens on a hot surface as liquid boils could help to enhance this process actively, and also avoid unexpected hotspots on surfaces which result in serious accidents and disable equipment.

Introduction to boiling characteristics

Boiling can be characterized by a boiling curve which was firstly reported by Nukiyama [5] in 1930s. Figure 1.6 shows a classical boiling curve which includes four regimes, i.e., natural convection, nucleate boiling, transition boiling and film boiling.

At the initial stage when the superheat is small, no bubbles nucleate on surfaces, while a thermal boundary layer forms adjacent to the surface with liquid locally heated. Then heat is transferred from the surface to the liquid by natural convection. If increasing the surface superheat to a certain degree, some sites, e.g., cavities, scratches and other imperfections, can be activated with bubble occurrence, and this superheat is called the onset of nucleate boiling (ONB). The nucleate boiling regime starts from ONB.

In the nucleate boiling regime, two distinguished bubble visualizations are recognized. One is the isolated bubble region where isolated bubbles nucleate on surfaces and depart. The other is the bubble column region with increasing superheats, where dense bubbles nucleate and coalesce intensively. In the natural convection and nucleate boiling regimes, heat fluxes increase with increasing superheats. However, there exists a critical heat flux beyond which a transition boiling regime occurs, because the amount of liquid that vaporizes on surfaces cannot be supplemented effectively.

In the transition boiling regime, heat fluxes decrease with increasing superheats, resulting in considerable heat transfer deterioration. For further increasing superheats, a film boiling regime appears. It should be noted that the transitional boiling regime only exists in a surface-temperature-controlled case, while in a heat-flux-controlled case, the transitional boiling regime does not occur and the nucleate boiling regime directly transits to the film boiling regime with increasing heat flux.

In the film boiling regime, surfaces are covered with superheated vapors. The heat transfer in this regime mostly depends on radiation and heat conduction, instead of bubble nucleation. Normally, this regime brings large surface superheats which are unacceptable in practical applications.

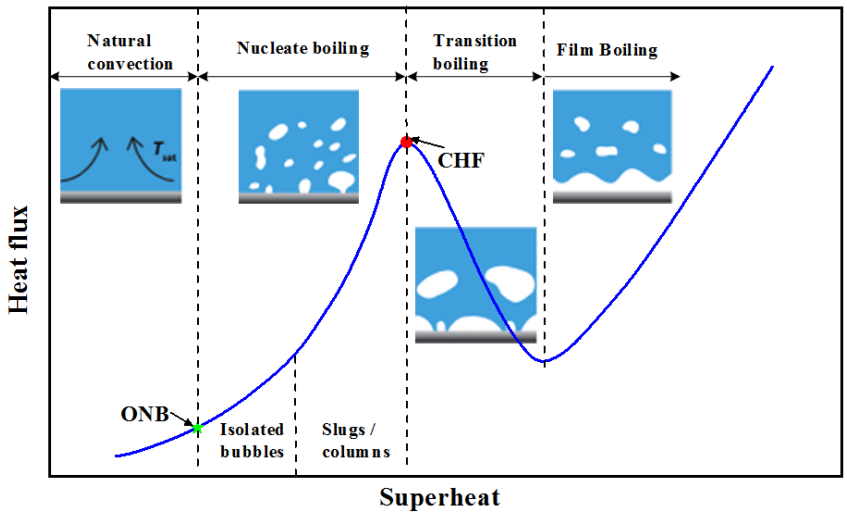

Figure 1.6: Boiling curve in a surface-temperature-controlled case [5].

1.2 Objectives and methodologies

As described above, boiling heat transfer is widely used in industrial sectors, and the nucleate boiling provides high heat transfer coefficients with low superheats in comparison to other boiling regimes. In addition, critical heat flux is a crucial parameter that indicates a dangerous condition in practical applications. Accordingly, the present thesis targets at the nucleate boiling heat transfer, including both heat transfer coefficient and critical heat flux.

Extensive studies have been carried out on topics related to nucleate boiling over last several decades, e.g., bubble nucleation including bubble growth and departure, heat transfer mechanisms and critical heat flux mechanisms. Even though significant progresses have been achieved, investigations are still required to get it clearer. In general, imperfections on surfaces that can trap gases/vapor, as nucleation embryo, have priority to nucleate bubbles. Therefore, surfaces with more active imperfections can enhance nucleate boiling. Nowadays,

with progresses of manufacturing technologies, especially micro/nano technologies, numerous enhanced surfaces have been developed to augment nucleate boiling.

In this thesis, nanoparticle-coating surfaces, microporous surfaces and hybrid micro/nano surfaces were prepared. Accordingly, nucleate boiling heat transfer was experimentally studied on these surfaces through pool boiling test facilities. The following objectives were initially setup:

- Comparatively study the effects of nanoparticle coatings, microporous coatings and hybrid micro/nano structures on nucleate boiling, using different liquids including dielectric liquids, organic liquids and water.
- Predict nucleate boiling heat transfer on the prepared surfaces by developing heat transfer models and correlations based on existing ones to some extent. Meanwhile, bubble dynamics, especially departure bubble diameter, should be investigated by high speed visualizations, and compared with bubble diameter models in literature.
- Explore possible mechanisms to trigger critical heat flux, referring to high speed visualizations. Try to improve existing critical heat flux models to obtain better prediction for the prepared surfaces.

However, this thesis does not involve works on bubble nucleation very much, especially bubble nucleation on a single nucleation site. In fact, single bubble nucleation is also important, which can help to understand physics of boiling better, and the related studies are still rare. This is one of possible future works.

1.3 Outline of the thesis

The thesis has 5 chapters. Chapter 1 introduces the background of the present study and basic knowledge on this topic. Chapter 2 provides a state-of-art literature review on the nucleate boiling heat transfer, including mechanistic heat transfer models, heat transfer correlations, critical heat flux models and enhanced surfaces. Chapter 3 gives the introduction to the surface preparations, pool boiling test facilities, experiments and data reduction. Chapter 4 summarizes the results and provides discussion. Chapter 5 ends up with conclusions and future outlook.

CHAPTER 2

State-of-the-Art Literature Review

Boiling is a complicated and seemingly chaotic process which makes its physical characteristics still vague. This chapter reviews the nucleate boiling, including heat transfer and critical heat flux, showing the progresses in the past decades. The heat transfer part includes bubble nucleation theories, mechanistic heat transfer models and heat transfer correlations, while the critical heat flux part introduces typical triggering mechanisms in the literature.

2.1 Bubble nucleation theory

As introduced previously, bubble nucleation is divided into homogeneous nucleation and heterogeneous nucleation. In this thesis, the nucleation discussed below is limited to the heterogeneous one.

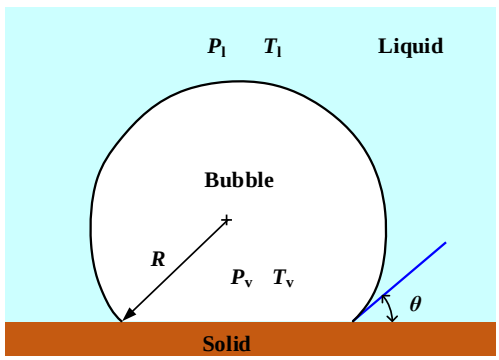

Figure 2.1: Bubble nucleation on idealized surface.

Assuming a vapor embryo existing on a perfectly smooth surface, as shown in Fig. 2.1, availability or Gibbs energy analysis can be carried out to decide conditions under which the embryo grows spontaneously or collapses. This has been presented representatively by Cole

[6], Wu et al. [7] and Quan et al. [8]. In general, the availability in the system shown in Fig. 2.1 can be derived as

$$E = \Delta G + \frac{1}{3}\pi R^2 \sigma_{\mathrm{lv}}(2 + 3\cos\theta - \cos^3\theta) \tag{2-1}$$

If the embryo is able to grow spontaneously, the embryo's Gibbs free energy should be less than or equal to the liquid's Gibbs free energy ($\Delta G <= 0$). Accordingly, Wu et al. [7] and Quan et al. [8] derived a critical embryo radius (R_e) with $\Delta G = 0$. Only embryos with larger radii than the critical one are able to nucleate. In the system with effective embryos, the availability is expressed as

$$E = \frac{1}{3}\pi R_e^2 \sigma_{\mathrm{lv}}(2 + 3\cos\theta - \cos^3\theta) \tag{2-2}$$

Equation (2-2) tells that the availability for nucleation is related to the contact angle. The availability tends to zero with $\theta = 0$, while it is maximum for $\theta = 180°$. This means that bubbles prefer to nucleate on hydrophobic surfaces. However, even though, this thermodynamic analysis explains why it is easy to nucleate on hydrophobic surfaces, it still cannot account for the much lower superheats found in practical situations. This is probably due to the presence of imperfections, e.g., cavities on the surfaces. Accordingly, nucleation in a cavity needs to be investigated.

In 1950s, basic studies on bubble nucleation in a cavity were carried out by Courty [9], Griffth and Wallis [10], and Bankoff [11], but these studies were based on isothermal conditions, saying that superheated liquid temperatures nearby walls were assumed equal to the wall temperature, which probably deviate from the physics. Hsu [12] is apparently the first one to investigate heterogeneous nucleation in a cavity, considering a liquid temperature gradient close to the wall.

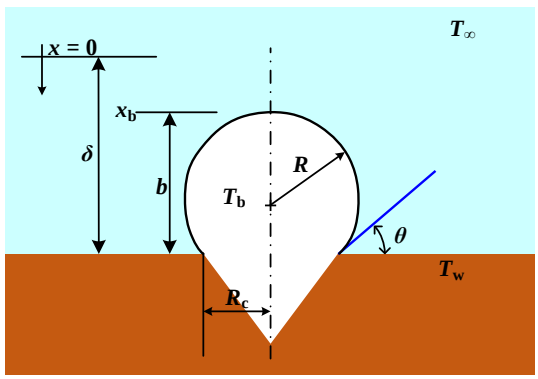

b =C_1R_c, R= C_2R_c, b=C_3R

C_1=(1+cosθ)/sinθ, C_2=1/sinθ, C_3=(1+cosθ)

Figure 2.2: Bubble nucleation in a cavity.

Hsu [12] proposed a theory of bubble nucleation, assuming transient conduction in the liquid nearby the wall, based on which, active nucleation site size and onset of nucleate boiling were

derived. The schematic of the bubble nucleation is shown in Fig. 2.2. It is postulated in this case that heat is transferred from the wall to the adjacent liquid by transient heat conduction and a thermal boundary layer is growing. This process happens in the waiting time of an ebullition cycle. However, the thickness of the thermal boundary layer cannot be infinite and beyond a certain value, the liquid temperature is constant as T_∞. Then, the liquid temperature profile can be analytically described by one-dimensional transient heat conduction with specific initial conditions and boundary conditions. The transient heat conduction is represented as

$$\frac{\partial(T-T_\infty)}{\partial t} = \alpha\left[\frac{\partial^2(T-T_\infty)}{\partial x}\right] \tag{2-3}$$

The corresponding solution is shown as [12]

$$\frac{T-T_\infty}{T_\mathrm{w}-T_\infty} = \frac{x}{\delta} + \frac{2}{\pi}\sum_{n=1}^{\infty}\frac{\cos n\pi}{n}\sin\left(n\pi\frac{x}{\delta}\right)e^{-n^2\pi^2 t} \tag{2-4}$$

Regarding nucleation conditions, it is supposed that bubble nuclei start to grow when the surrounding liquid is at a temperature above or equal to the temperature of bubbles, and the bubble temperature can be derived from the Clausius-Clapeyron equation and the Laplace equation, which can be described as

$$T_\mathrm{b} = T_\mathrm{sat} + \frac{2\sigma_\mathrm{lv}T_\mathrm{sat}}{i_\mathrm{lv}\rho_\mathrm{v}R} = T_\mathrm{sat} + \frac{2\sigma_\mathrm{lv}T_\mathrm{sat}}{i_\mathrm{lv}\rho_\mathrm{v}\left(\frac{\delta-x_\mathrm{b}}{C_3}\right)} \tag{2-5}$$

A cavity is effective when the temperature profile from Equation (2-4) can intersect with that from Equation (2-5), and the critical cavity size can be derived from the intersection points when *t* approaches infinity in Equation (2-4). Then the effective cavity size range is formulated as

$$R_\mathrm{c,min/max} = \frac{\delta}{2C_1}\left[1-\frac{T_\mathrm{sat}-T_\infty}{T_\mathrm{w}-T_\infty} \pm \sqrt{\left(1-\frac{T_\mathrm{sat}-T_\infty}{T_\mathrm{w}-T_\infty}\right)^2 - \frac{4C_3}{\delta(T_\mathrm{w}-T_\infty)}\cdot\frac{2\sigma_\mathrm{lv}T_\mathrm{sat}}{i_\mathrm{lv}\rho_\mathrm{v}}}\right] \tag{2-6}$$

Referring to Equation (2-6), the incipient boiling occurs at the condition that

$$\left(1-\frac{T_\mathrm{sat}-T_\infty}{T_\mathrm{w}-T_\infty}\right)^2 - \frac{4C_3}{\delta(T_\mathrm{w}-T_\infty)}\cdot\frac{2\sigma_\mathrm{lv}T_\mathrm{sat}}{i_\mathrm{lv}\rho_\mathrm{v}} = 0 \tag{2-7}$$

Han and Griffith [13] carried out an analysis of bubble nucleation with much the same idea as Hsu [12], but the transient heat conduction was solved with different initial and boundary conditions and a different bubble shape was set up.

$$\frac{T-T_\infty}{T_\mathrm{w}-T_\infty} = \mathrm{erfc}\frac{x}{2(\alpha t)^{1/2}} \tag{2-8}$$

It was assumed that the temperature varied linearly in the thermal boundary layer, and the waiting time of bubble nucleation was thought to end when the liquid temperature at a distance of 1.5 R_c from the wall is equal to the bubble temperature derived by combining the Clausius-Clapeyron equation and the Laplace equation. Then the effective cavity size range is formulated as

$$R_{\mathrm{c,min/max}} = \frac{\delta}{3}\frac{T_{\mathrm{w}}-T_{\mathrm{sat}}}{T_{\mathrm{w}}-T_{\infty}}\left[1 \pm \sqrt{1-\frac{12(T_{\mathrm{w}}-T_{\infty})}{\delta(T_{\mathrm{w}}-T_{\mathrm{sat}})^2}\cdot\frac{\sigma_{\mathrm{lv}}T_{\mathrm{sat}}}{i_{\mathrm{lv}}\rho_{\mathrm{v}}}}\right] \tag{2-9}$$

2.2 Heat transfer mechanism

Nucleate boiling is a complex process which is a multi-physics (mass and heat transfer) and multi-phase (vapor, liquid and solid) topic and even now its physics is still not well understood. Until now, great efforts have been taken to study mechanisms of the nucleate boiling and progresses have been achieved.

Initially, Forster and Zuber [14] and Rohsenow [15] attempted to analyze the nucleate boiling by postulating that heat transfer between walls and adjacent liquids was similar to a single-phase convection, and the high heat transfer coefficient was dependent on local agitation due to bubble dynamics. Afterwards, Tien [16] developed a hydrodynamic model for the nucleate boiling, considering the induced flow associated with a rising bubble column as an inverted stagnation flow. These works help to understand the nucleate boiling to some extent, but obviously liquid-vapor transformation was not considered. Therefore, mechanistic work is required. In fact, with progresses on this topic, a few mechanistic models were proposed.

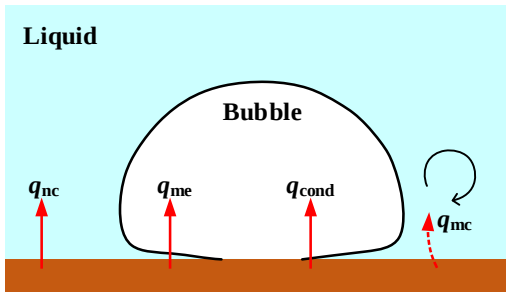

Figure 2.3: Schematic of heat transfer mechanisms.

Figure 2.3 shows a schematic of possible heat transfer mechanisms which include heat transfer by natural convection, transient heat conduction, microlayer evaporation and transient micro-convection. In general, the natural convection is due to a difference of liquid densities between inside and outside the thermal boundary layer, which occurs in an uninfluenced region, while other items take place in an influenced region with a diameter twice of the bubble departure diameter, as suggested by Han and Griffith [17], and Mikic and Rohsenow [18]. The transient heat conduction appears as the thermal boundary layer is reformed when a bubble departs and new cold liquid rushes onto the wall. The microlayer evaporation is the latent heat related to a microlayer beneath the bubble. The transient micro-convection is a result of convection in the wake of departing bubbles. In fact, it is easy to estimate q_{nc} only with superheats and liquid properties, but it is tricky to estimate the others, and corresponding efforts will be reviewed in the following sections.

Transient heat conduction

Han and Griffith [17] assumed that the liquid temperature varies linearly within the thermal boundary layer and the thickness of thermal boundary layer increases linearly along the radial direction. Accordingly, heat transfer due to the transient heat conduction is estimated as the increasing rate of internal energy

$$q_{\mathrm{cond}} = \frac{1}{2}\rho_{\mathrm{l}} C_{\mathrm{pl}} (T_{\mathrm{w}} - T_{\infty}) f \left[D_{\mathrm{i}}^2 \delta_{\mathrm{d}} - \frac{1}{3} D_{\mathrm{d}}^2 (\delta_{\mathrm{d}} - \delta_{\mathrm{w}}) \right] Na \tag{2-10}$$

Mikic and Rohsenow [18] assumed that pure conduction occurs in the influenced area during the whole bubble cycle, while the conduction was modeled for a semi-infinite body. Then, a new formula was suggested

$$q_{\mathrm{cond}} = 2\sqrt{\pi} \sqrt{\left(\rho k C_{\mathrm{p}}\right)_{\mathrm{l}}} \sqrt{f} D_{\mathrm{d}}^2 (T_{\mathrm{w}} - T_{\infty}) Na \tag{2-11}$$

However, Benjamin and Balakrishnan [19] pointed out that only pure conduction occurs in the influenced area during the waiting time (t_{w}) instead of the whole bubble cycle, then

$$q_{\mathrm{cond}} = 2\sqrt{\pi} \sqrt{\left(\rho k C_{\mathrm{p}}\right)_{\mathrm{l}}} \sqrt{\frac{1}{t_{\mathrm{w}}}} D_{\mathrm{d}}^2 (T_{\mathrm{w}} - T_{\infty}) Na \tag{2-12}$$

Microlayer evaporation

A microlayer is a superheated liquid layer beneath a bubble. It is assumed that latent heat from the microlayer evaporation contributes to the bubble growth. Guo and El-Genk [20] numerically studied the microlayer evaporation on a surface of a flat composite wall and concluded that the rate of microlayer evaporation increased with increasing thickness and thermal conductivity of the wall. However, a general formula to calculate q_{me} can be simply expressed as

$$q_{\mathrm{me}} = \rho_{\mathrm{l}} V_{\mathrm{me}} i_{\mathrm{lv}} f Na \tag{2-13}$$

Therefore, it is essential to estimate the volume of the microlayer. However, to the knowledge of the author, no studies can describe the microlayer exactly, although some works are available. Sernas and Hooper [21] experimentally studied the initial vapor growth on a wall and postulated a microlayer of constant thickness underlying a bubble based on a comparison with five analytical models. Copper and Lloyd [22] predicted the microlayer thickness by a simplified hydrodynamic theory, indicating that the thickness is linear to the root of the growth time. Voutsinos and Judd [23] investigated the microlayer evaporation by laser interferometry and then derived an expression of the microlayer volume. Benjamin and Balakrishnan [19] and Li et al. [24] suggested an estimation of the microlayer volume by considering an energy balance in the microlayer. With more and more advanced measurement techniques, like the utilization of transmission electron microscope (TEM) and atomic force microscope (AFM), more details in micro/nanoscale can be expected in the future.

Transient micro-convection

Haider and Webb [25] developed a transient micro-convection model of nucleate pool boiling, based on that of Mikic and Rohsenow [18]. The transient micro-convection was due to the convection in the wake of a departing bubble. It was formulated that the transient heat conduction prevails in the initial phase of a bubble cycle and then convective effects become important. An asymptotic correlation is proposed to patch the transient conduction and transient micro-convection, which is described as

$$q_{\mathrm{cond}} + q_{\mathrm{mc}} = 2\sqrt{\pi \cdot f \cdot k_{\mathrm{l}} \cdot \rho_{\mathrm{l}} \cdot C_{\mathrm{pl}}}\, D_{\mathrm{d}}^{2} (T_{\mathrm{w}} - T_{\mathrm{sat}}) \cdot \left[1 + \left(\frac{0.66\pi c}{\mathrm{Pr}_{\mathrm{l}}^{1/6}}\right)^{m}\right]^{\frac{1}{m}} Na \qquad (2\text{-}14)$$

As reviewed above, numerous mechanistic models have been developed to study nucleate boiling heat transfer. However, these models require many parameters, like bubble departure diameters, bubble departure frequencies and active nucleation site densities, which are hard to obtain, especially the active nucleation site densities. Alternatively, heat transfer correlations are good options to study the nucleate boiling heat transfer, like the Stephan and Abdelsalam correlation [26], the Nishikawa correlation [27], the Cooper correlation [28], the Gorenflo and Kenning correlation [29], the Leiner correlation [30] and the Ribatski and Jabardo correlation [31]. Hundreds and thousands of data, covering different liquids, different pressures and different boiling surfaces, were correlated in the development of these correlations.

Surely, the review above cannot incorporate all relevant studies. Literature reviews such as Kim [32] and Mohanty and Das [33] are recommended for supplement, regarding nucleate boiling heat transfer mechanisms and correlations.

2.3 Critical heat flux mechanism

The critical heat flux describes a safety threshold, beyond which heat transfer coefficients will decrease dramatically. Imaging that the critical heat flux occurs in practical application, surfaces subjected to heat transfer will be in a dangerous situation, with unacceptable temperature overshoots, probably resulting in accidents, e.g., burn-out of equipment. Therefore, it is essential to study the critical heat flux, knowing its physics and avoiding to surpass it in reality. Roughly speaking, the critical heat flux takes place when vapor accumulates on surfaces and liquid cannot rewet the surfaces anymore. Therefore, this is a physical phenomenon involving vapor, liquid and solid, making its physics complicated. To the best knowledge of the author, even though extensive investigations have been conducted on the critical heat flux and several mechanisms were proposed accordingly, still no universal mechanisms are accepted. In the following, some representative critical heat flux mechanisms are reviewed.

Zuber [34] proposed a mechanism to trigger critical heat flux, from the perspective of hydrodynamic instabilities. Figure 2.4 indicates the idea about the critical heat flux due to hydrodynamic instabilities. As is known, Taylor instability occurs when a lighter fluid is

pushing a heavier fluid. Regarding the flow condition at critical heat flux, it can be imagined that the vapor pushes the liquid, preventing the liquid from rushing onto the surface. Therefore, the Taylor instability appears in this flow condition. Zuber also assumed that the vapor departs from surfaces, with a shape of column which has a diameter half of the instability wavelength, and the liquid flows between columns towards surfaces. In addition, due to the slippery velocity between the vapor and the liquid, the Helmholtz instability takes place as well, which causes coalescence of adjacent vapor columns with the instability growth. Critical heat flux is thought to occur when the coalescence vapor collapses on surfaces and the Helmholtz instability reaches a critical condition. Therefore, critical heat flux can be predicted quantitatively, related to the hydrodynamic instabilities, and is expressed as

$$\frac{\mathrm{CHF}}{\frac{\pi}{24}\rho_{\mathrm{v}}^{1/2} i_{\mathrm{lv}}[\sigma g(\rho_{\mathrm{l}}-\rho_{\mathrm{v}})]^{1/4}} = \left(\frac{3}{\sqrt{2\pi}}\frac{1}{3^{1/4}}, \frac{3}{\sqrt{2\pi}}\right) \tag{2-15}$$

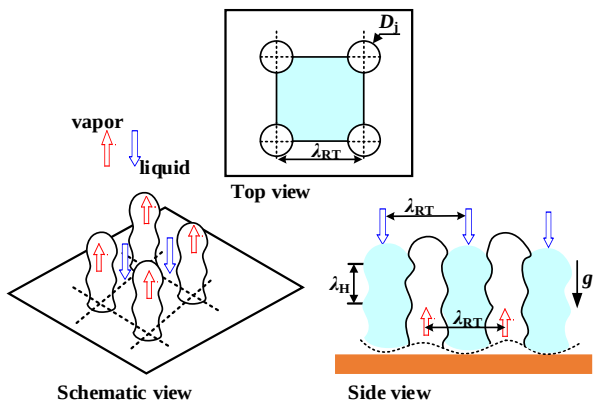

Figure 2.4: Illustration of Zuber's hydrodynamic instability model.

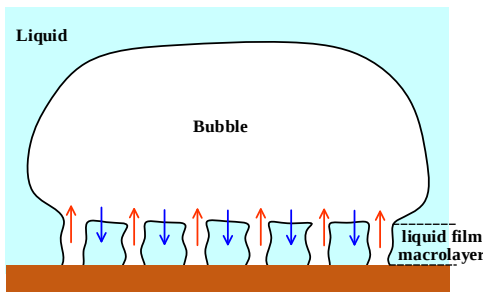

Figure 2.5: Schematic of Haramura and Katto's model.

Later on, Haramura and Katto [35] proposed a new hydrodynamic model of critical heat flux, following some observations from experiments. The model is normally called macrolayer dryout model. A liquid film layer was considered beneath large bubbles, as shown in Fig. 2.5. An analysis was conducted, considering hydrodynamic instabilities and bubble dynamics. Critical heat flux occurs when the liquid film is not supplied with liquid from the bulk region during the period that large bubbles hover on the liquid film.

Yagov [36] discussed contradictions and limitations of the hydrodynamic theory and proposed a new mechanism that triggers critical heat flux. In this mechanism, it is considered that the critical heat flux is related to the dry spot area beneath bubbles. Critical heat flux appears when the liquid evaporates faster than liquid supplement around dry spots, and the critical dry spot size is proportional to bubble departure diameter. The concept of dry spot area beneath bubbles was validated experimentally by Chu et al. [37]. The experiments indicate that two types of dry spots exist, i.e., reversible spots and irreversible spots, and the dry spot size evolves periodically at critical heat flux, but it is assumed to increase monotonically in Yagov's model. Then, Zhao and Williams [38] developed a new critical heat flux model based on irreversible dry spots.

Guan et al. [39] further emphasized the observation of dry spots (vapor patches) by hundreds of video sequences. Consistent with Haramura and Katto [35], a liquid macrolayer beneath bubbles was also considered. However, Guan et al. postulated that critical heat flux occurs when the liquid layer is lifted by vapor patches. Figure 2.6 shows the schematic of the model. Critical heat flux was formulated with critical heat flux vapor velocity which was derived by an analysis of momentum conservation. The final formula is

$$\mathrm{CHF} = 0.2445\rho_{\mathrm{v}} i_{\mathrm{lv}} \left[\frac{\sigma g(\rho_{\mathrm{l}}-\rho_{\mathrm{v}})}{\rho_{\mathrm{v}}^2}\right]^{1/4} \left(1+\frac{\rho_{\mathrm{v}}}{\rho_{\mathrm{l}}}\right)^{1/4} \left(\frac{\rho_{\mathrm{v}}}{\rho_{\mathrm{l}}}\right)^{1/10} \tag{2-16}$$

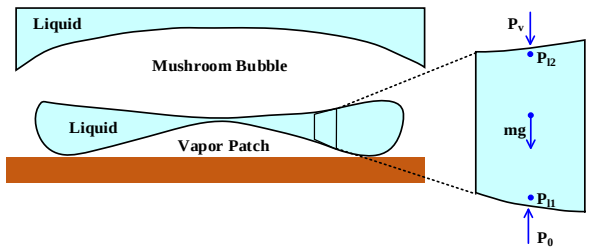

Figure 2.6: Schematic of Guan's lift-off model.

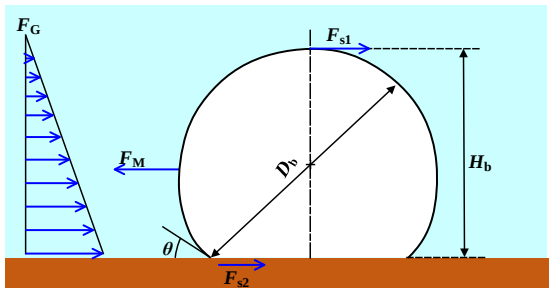

Figure 2.7: Schematic of Kandlikar's model.

Kandlikar [40] derived a theoretical model based on a force analysis, emphasizing the importance of receding contact angles. The considered forces include a momentum force due to liquid evaporation, surface tension forces at the bubble base and at the bubble top surface, and a force due to gravity, as shown in Fig. 2.7. Accordingly, critical heat flux is triggered

when the momentum force exceeds the sum of other forces. The momentum force pulls the bubble along the surface, pushing the liquid away from the surface, while other forces hold the bubble. Finally, a formula is suggested as

$$\mathrm{CHF} = i_{\mathrm{lv}}\rho_{\mathrm{v}}^{1/2} \cdot [\sigma(\rho_{\mathrm{l}} - \rho_{\mathrm{v}})g]^{1/4} \cdot \frac{1+\cos\theta_{\mathrm{rec}}}{16} \cdot [\frac{2}{\pi} + \frac{\pi}{4}(1+\cos\theta_{\mathrm{rec}})]^{1/2} \quad (2\text{-}17)$$

Definitely, the critical heat flux has been studied extensively in the past, including the effect of wettability, surface roughness and liquid-spreading ability, but most studies are extensions of the mechanisms reviewed above. For example, a model considering the effect of liquid wicking was developed by Rahman et al. [41] based on the Zuber's model, and the Kandlikar's model was also further developed by Chu et al. [42] and Quan et al. [43], but these models are not reviewed in details. Recently, Ding et al. [44] innovatively derived the critical heat flux mathematically with a concept of microscopic "film boiling", considering a bubble nucleation process, but this is not discussed in details neither. In addition, a review of critical heat flux mechanisms by Liang and Mudawar [45] is recommended.

2.4 Enhanced boiling surfaces

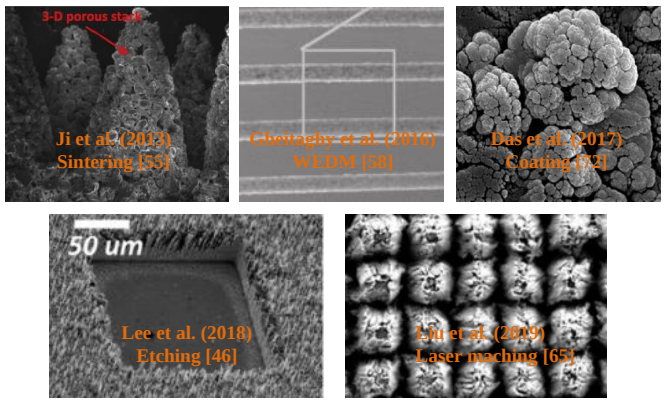

Figure 2.8: Demonstration of representative enhanced surfaces in literature.

Enhancement of nucleate boiling has been a hot topic. As reviewed above, the nucleate boiling, including bubble nucleation, heat transfer and critical heat flux, is dependent on surface characteristics. Modifications of surfaces are supposed to enhance the nucleate boiling performance. Accordingly, many enhanced boiling surfaces were developed in the past with different micro/nano fabrication technologies, e.g., etching, sintering, wire electric discharge machining, laser machining, and coating techniques. Figure 2.8 demonstrates some enhanced surfaces in literature, prepared by different techniques. A brief review about the enhanced boiling surfaces is presented following.

Etching

The etching method is commonly used to fabricate structures on silicon wafers. Lee et al. [46] prepared micro-structure (cavity) surfaces by dry etching, nano-structure (nano wire) surfaces

by reactive-ion etching and hybrid micro/nano-structure surfaces by combining these two methods, respectively. Pool boiling of water was comparatively studied on the prepared surfaces and the results show that nucleate boiling performance is enhanced on the three types of surfaces, but the hybrid surfaces perform the best. Similarly, Moon et al. [47] experimentally studied pool boiling of water on silicon surfaces with micro pillars, micro holes and composite micro-nano structures, prepared by etching. It was found that the surface with micro pillars and nanowires achieved the highest critical heat flux, which was due to a capillary pressure potential through forming a curved liquid meniscus on the pillar structures. Kim et al. [48] fabricated a set of micro-pillar surfaces with different micro pillars diameter, gap and diameters, using deep reactive-ion etching. Experiments showed that both heat transfer and critical heat flux were enhanced. The increasing heat transfer was attributed to the extended heat transfer area, while the increasing critical heat flux is due to the improved capillary wicking rate. Dhillon et al. [49] especially studied critical heat flux of water on micro-pillar surfaces and nano-structure surfaces prepared by etching. Liquid imbibition experiments and quantitative infrared temperature measurements of dry spots on the surfaces were carried out, which provided direct evidence that the critical heat flux was dictated by characteristic dry spot heating and rewetting timescales. Kim et al. [50] experimentally studied interfacial wicking dynamics and its impact on critical heat flux, on surfaces with nano-pillars prepared by nanosphere lithography combined with top-down metal-assisted chemical etching. The results revealed that strong wicking can guarantee hydrodynamic stability against dryout, therefore enhancing critical heat flux. Wei et al. [51] studied pool boiling of FC-72 on micro-pin-fin surfaces prepared by dry etching, achieving enhanced results.

Sintering

Lie and Peterson [52] fabricated surfaces with sintered copper mesh and tested the effect of mesh size and porosity on pool boiling of water. The experimental results indicated that the critical heat flux (CHF) was strongly dependent on both the mesh size and the volumetric porosity; while the evaporation/boiling heat transfer coefficient was significantly affected by mesh size, but not strongly dependent on the volumetric porosity. Min et al. [53] experimentally studied pool boiling of pentane on copper surfaces with 2-D and 3-D modulated porous coatings prepared by sintering, while the coatings had different height, width and pitch. It was found that the coating can considerably enhance the boiling performance and the critical heat flux can be well predicted by a hydrodynamic stability model originating from the Zuber's model. Cora et al. [54] tried to find proper conditions (temperature and pressure) and procedures (sintering after compactions and compaction after sintering) for robust, low-cost mass manufacturing of microporous structures for heat transfer applications. Through pool boiling experiments, sintering after compactions, with low pressures, was recommended to produce microporous and modulated surface layers bonded to a solid substrate. Ji et al. [55] also developed uniform and non-uniform coating surfaces by sintering and studied pool boiling of acetone on the surfaces. Heat transfer and critical heat flux were enhanced by the coatings, and a hollow well exposed in liquid was captured at critical heat flux by high speed visualization. Liquid was supposed to rewet the surfaces

through the hollow well. Pastuszko and Wojcik [56] investigated pool boiling of water and FC-72 on micro-fin surfaces with a sintered perforated foil, with a comparison to a smooth surface and micro-fin surfaces without foil. It was found that micro-fin surfaces with sintered perforated foil provided the highest heat transfer coefficients and critical het flux, and the critical heat flux was increased by 130% and 75% for water and FC-72, respectively, in comparison to the smooth surface.

Wire electric discharge machining (WEDM)

Das et al. [57] prepared surfaces having a number of parallel channels or orthogonally channels by WEDM, and pool boiling experiments were conducted with water. It was found that the highest augmentation was achieved on surfaces with intersecting inclined channels with a circular base. Gheitaghy et al. [58] employed WEDM and an electrochemical deposition method to fabricate mesochannel surfaces, microporous surfaces and combined surfaces. The results showed that boiling performance of water can be enhanced by the two methods, but the surfaces combining the two methods performed the best. Tang et al. [59] studied pool boiling of water on surfaces modified by WEDM, sintering and combined method, respectively, and the effects of powder morphology, powder size and channel width on the heat transfer were compared. Similarly, Akbari et al. [60]studied the effect of silver nanoparticle deposition on pool boiling enhancement on re-entrant inclined minichannel prepared by WEDM. As a consequence, the combined modification including a coating and minichannel possessed the highest heat transfer coefficient and critical heat flux. Sun et al. [61] investigated pool boiling performance and bubble dynamics on microgrooved surfaces with re-entrant cavities. It was found that the wall superheat at the onset of nucleate boiling was lower on the prepared surfaces and the heat transfer coefficient was enhanced. However, the critical heat flux was not reached in the experiments due to limitations of the experimental setup.

Laser machining

Kruse et al. [62] used femtosecond laser to process stainless steel surfaces, aiming to enhance pool boiling heat transfer and critical hat flux. The results showed that the heat transfer coefficient and critical heat flux were enhanced by 200% and 60% in water, respectively, in comparison to a smooth surface. The critical heat flux enhancement was due to the wetting and wicking ability, while the heat transfer enhancement was due to the increased surface area and nucleation site density. Ho and Leong [63] studied pool boiling of FC-72 on enhanced aluminum surfaces produced by selective laser melting. The enhanced surfaces presented considerable enhancement in heat transfer (70% augmentation) and critical heat flux (76% augmentation), compared with a smooth surface. Wong and Leong [64] also used selective laser melting to produce porous lattice structures to enhance pool boiling performance of FC-72, and the enhancement was attributed to the increased surface area, increased nucleation site density and capillarity-assisted suction of the porous structure. Liu et al. [65] experimentally investigated pool boiling of FC-72 on structured silicon surfaces fabricated by femtosecond laser, and reported a “hook back” phenomenon on the structured surfaces. Recently, Zhang et al. [66] designed and manufactured 3D grid structures on stainless steels,

using selective laser melting technique. Pool boiling of water was tested on the structured surfaces, which showed that the grid structures can significantly influence nucleate boiling behavior and enhance critical heat flux. The enhancement of critical heat flux was a result of the grid structure's "partition effect" that inhibits Helmholtz instability and confines hot spots expansion.

Coating techniques

Numerous techniques are employed to generate coatings on surfaces, e.g., electrophoretic deposition, chemical/physical vapor deposition, electrochemical deposition, sputtering and electron beam evaporation technique. White et al. [67] modified stainless steel surfaces by electrophoretic deposition of nanoparticles from a nanofluid. Pool boiling experiments of water illustrated an enhancement of 200% in heat transfer coefficient. Jun et al. [68] experimentally and theoretically studied pool boiling of water and ethanol on copper surfaces covered with copper-plating nanofibers, prepared by electrospinning. The results showed that heat transfer coefficient was enhanced by 3-8 times, but critical heat flux was quite close to each other. Sahu et al. [69] covered copper surfaces with copper-plating polymer nanofibers by an electrically-assisted supersonic solution blowing process. Pool boiling of water, ethanol and their binary mixtures were tested. Heat transfer coefficient was considerably enhanced by the nanofibers. Pratik et al. [70] used an atmospheric pressure chemical vapor deposition process to deposit foam-like hierarchical hexagonal boron nitride nanomaterial on silicon surfaces and pool boiling of water was studied. The critical heat flux of the modified surface appeared comparable to that on a smooth surface, but the surface superheat at critical heat flux was reduced and correspondingly the heat transfer coefficient was increased. Das et al. [71, 72] utilized electron beam evaporation technique to coat copper surfaces with SiO_2 and TiO_2 nanostructures, and nucleate boiling heat transfer coefficient of water was compared between the nanostructured surfaces and a smooth surface, which indicated remarkably augmentation. The enhancement mechanisms involved surface area enlargement, more nucleation sites and enhanced surface wettability. Jo et al. [73] electroplated nickel-chrome wires with a pure copper layer and then annealed the wires, tuning the wettability by the electroplating time. Corresponding pool boiling of water was studied and analyzed. Gheitaghy [74], Wang et al. [75] and Rishi [76] deposited microporous coatings on copper surface by electrochemical deposition, which indicated effective nucleate boiling enhancement. Recently, Son and Kim [77] employed DC magnetron sputtering and arc-ion plating techniques to deposit coatings on surfaces, varying surface roughness and wettability and comparatively studied pool boiling of water on these surfaces. A critical heat flux model was developed, which is a function of roughness, surface area enlargement ratio and apparent contact angle, based on the mechanism of receding capillary flow, showing good prediction.

Some reviews are suggested for readers about interested in nucleate boiling surfaces, e.g., the review by Liang and Mudawar [78], by Kim et al. [79] and by Patil and Kandlikar [80].

CHAPTER 3

Surface Preparation and Test Rigs

In this chapter, the techniques used to modify surfaces are introduced, including an electrophoretic deposition method, an electrochemical deposition method, an electrostatic deposition method and femtosecond laser. Then, experimental setups, i.e., pool boiling test rigs and wettability measurements, as well data reduction are presented.

3.1 Surface preparation

In this thesis, smooth surfaces were prepared and tested first as a baseline for the comparison. The smooth surfaces were prepared by the following steps:

1) Polished with sandpapers of grit P220, P600, P1000, P1500 and P2000.
2) Cleaned by ultrasonic bath with acetone (20 mins) and ethanol (5 mins).
3) Immersed in H_2SO_4 0.5M for 2 hours.
4) Rinsed with water.

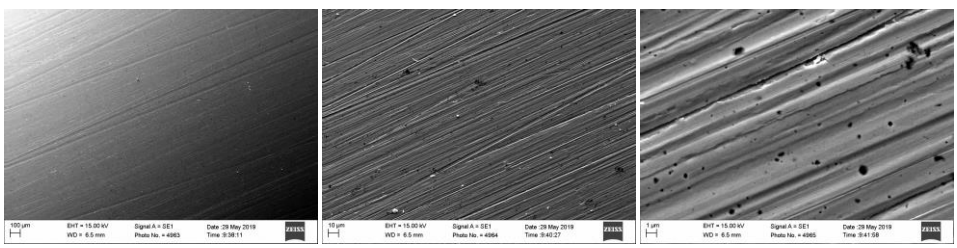

Figure 3.1: SEM images of a smooth surface.

Figure 3.1 shows the SEM images of a smooth surface. Some scratches exist due to the polishing by sandpapers. These scratches are likely to act as active nucleation sites. The roughness was measured on several smooth surfaces by a 3D optical profiler (Dektak 6M), ranging from around 60 nm to around 110 nm.

Surface modifications were implemented on smooth surfaces. Several techniques were attempted to modify the surfaces, including electrophoretic deposition, electrochemical deposition, electrostatic deposition and femtosecond laser. The setups for electrophoretic deposition and electrochemical deposition were constructed in our group, while the setups for electrostatic deposition and femtosecond laser were available in NanoLund and Xi'an Jiaotong University, respectively.

Electrophoretic deposition

Figure 3.2 indicates the schematic of the electrophoretic deposition process (EPD). With this method, two types of nanoparticles were used, namely copper nanoparticles (50 nm - 80 nm) and copper-zinc nanoparticles (~100 nm), both commercially available from Sigma-Aldrich Corporation. Firstly, nanoparticle dispersions were prepared by dissolving nanoparticles in DI water, with an ultrasonic bath for two hours. A certain volume of particle dispersion was dropped onto smooth surfaces sealed in a plastic tube by a pipette. Ethanol was then added to mix with the particle dispersion, obtaining a relatively uniform nanoparticle distribution. Two electrodes were set up and a potential of 9.5V (a DC power supply HP E3615A) was applied and remained for 30 minutes. The smooth surface was set as cathode for positively charged particles or anode for negatively charged particles. When the deposition ended, ethanol solution was gently removed from the plastic tube. The modified surface was put on a stirring hotplate (Fisherbrand) and heated at 75ºC (±5ºC) for 30 seconds to remove any excess liquid.

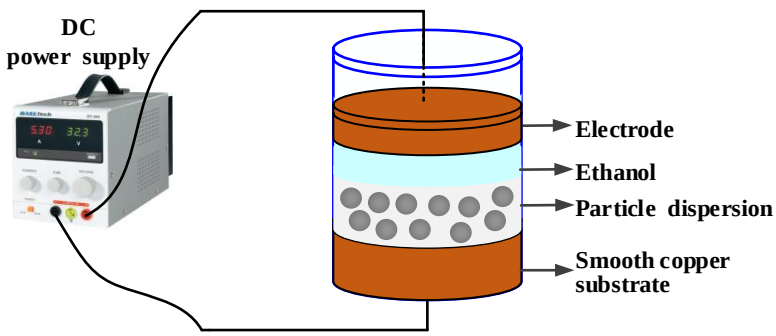

Figure 3.2: Schematic of the electrophoretic deposition process.

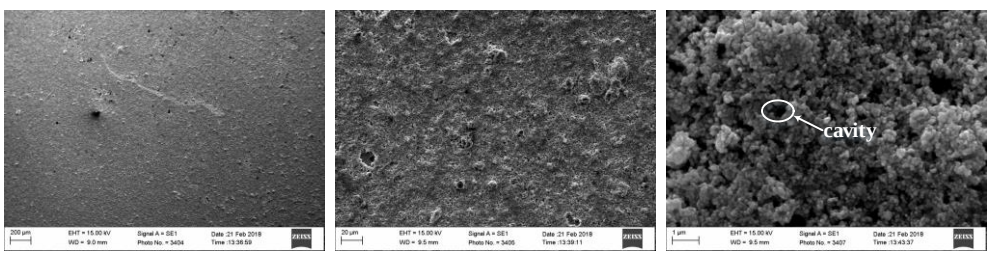

Figure 3.3: SEM images of a surface modified by the electrophoretic deposition method.

Figure 3.3 shows the SEM images of a surface deposited with 0.6 mg Cu-Zn nanoparticles, prepared by the electrophoretic deposition method. It is evident that a coating is formed on the surface, with nanoparticle clusters, generating numerous structures, e.g., pores, cavities and other irregularities. It is postulated that these structures are beneficial to boiling performance.

Electrochemical deposition

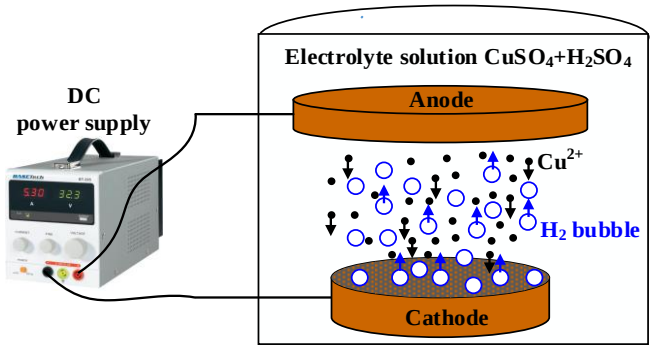

Figure 3.4: Schematic of the electrochemical deposition process.

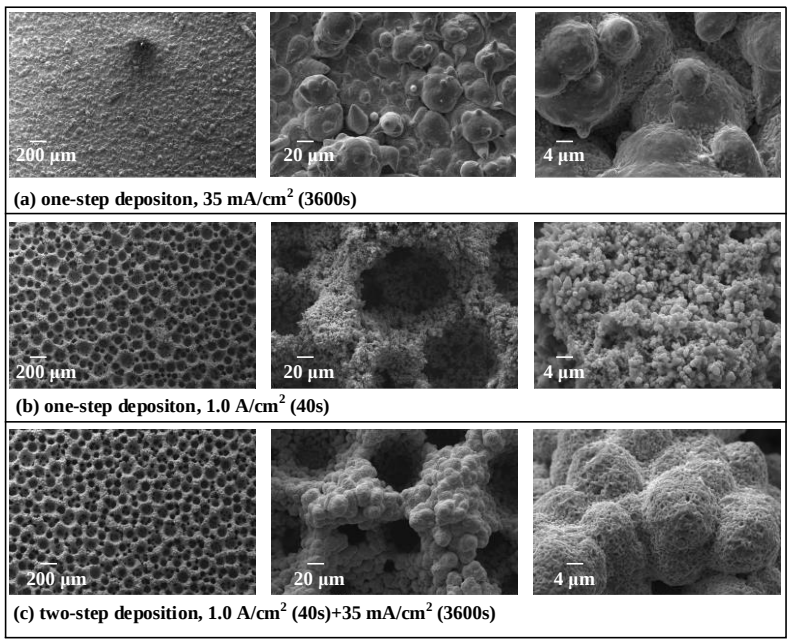

Figure 3.5: SEM images on surfaces by one-step deposition and two-step deposition.

Figure 3.4 indicates the schematic of the electrochemical deposition process (ECD). The principle is to reduce Cu^{2+} and H^+ ions on the cathode though a DC electrical field, as shown in the reactions in Equation (3-1). The reduction of Cu^{2+} ions generates porous coatings, while

the reduction of H^+ ions forms hydrogen gas which rises up, generating micro pores on the porous coatings. In this thesis, the electrolyte solution of $CuSO_4$ and H_2SO_4 was used. The concentration of sulfuric acid was fixed at 1.5 M, while the concentration of copper sulfate varied from 0.1 M to 0.4 M.

$$Cu^{2+} + 2e^{-1} = Cu, \quad 2H^+ + 2e^{-1} = H_2 \tag{3-1}$$

Generally, a two-step deposition strategy is widely selected, considering the stability and durability of coatings. However, in this thesis, the coating surfaces were prepared by a one-step deposition and a two-step deposition, respectively, considering different liquids. In the one-step deposition, either a large current density for a very short time or a very low current density for a long time was used, while in the two-step deposition, the first step was to deposit coatings, using a large current density for a very short time (several tens of seconds) and the second step was to further deposit coatings at a very low current density for a long time (one hour). After deposition, surfaces were annealed at 350 °C for one hour to make the deposition structure more stable.

Figure 3.5 compares the SEM images of surfaces prepared by one-step deposition and two-step deposition. In this case, the concentrations of $CuSO_4$ and H_2SO_4 were 0.4 M and 1.5 M, respectively. It is found that the morphology differs considerably among the surfaces. Regarding the surface with a low current density for a long time (Fig. 3.5(a)), a coating was formed on the surface with a relatively low porosity. Large particle clusters tightly connected with each other, generating some pits. Regarding the surface with a large current density for a short time (Fig. 3.5(b)), the coating had large porosity, with numerous micro pores generated by H_2 release and numerous smaller pores on structures among the micro pores. Regarding the surface combining the large and the small current densities (Fig. 3.5(c)), the coating was roughly similar to that in Fig. 3.5(b). However, the structures among micro pores were not that fluffy.

Electrostatic deposition

Compared with the two deposition techniques above, the system of electrostatic deposition is much more complex, which was carried out through a collaboration with NanoLund. In this thesis, the electrostatic deposition was especially used to deposit nanoparticles on silicon surfaces, which cannot be fulfilled by the two techniques above. Figure 3.6 presents the schematic of the electrostatic deposition process. Two opposing electrodes, as the seed material, are separated by a 2 mm gap and are charged until a spark arises. Material from the electrode is released and collides into agglomerates that are carried away by a continuous gas flow of 99.9999% pure N_2 at 1.68 lpm. The agglomerates are reshaped and compacted into spherical nanoparticles when the aerosol flow passes through the tube furnace at 1100 °C. Then the nanoparticles are size-selected using a differential mobility analyzer (DMA) in order to obtain a narrow size distribution of the nanoparticles. The size selected nanoparticles are deposited using an electrostatic precipitator (ESP). About 40% of the particles were deposited on the silicon surfaces, while the rest is deposited outside. The deposition was performed for several hours with a nanoparticle number concentration of 2000000 #/cm^3. As the

concentration of the nanoparticles on the surface increases, some larger clusters are formed due to the antenna effect. The antenna effect means the larger the clusters, the higher probability for the next particle to be deposited onto the cluster.

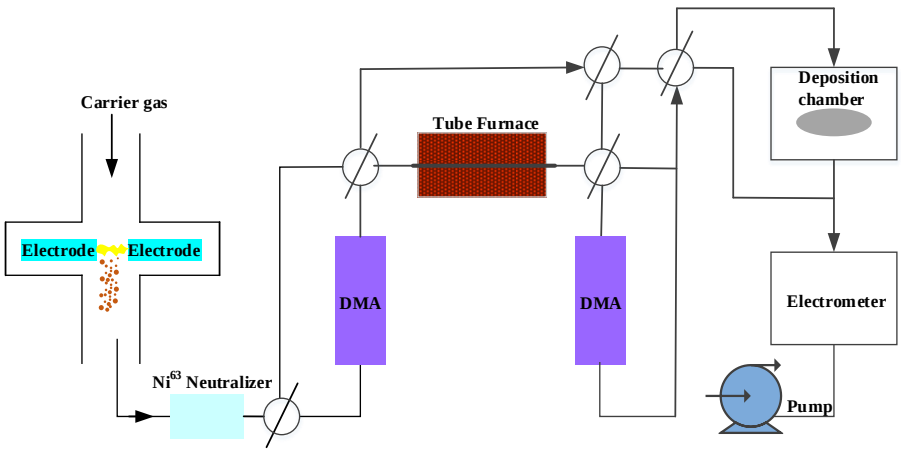

Figure 3.6: Schematic of the electrostatic deposition process.

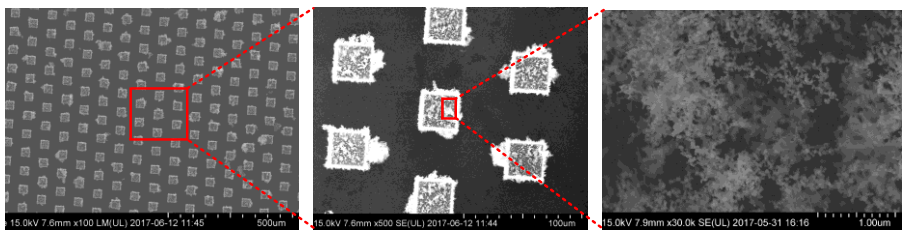

Figure 3.7: SEM images on a surface by electrostatic deposition.

Figure 3.7 shows the SEM images on a micro-pin-fin surface deposited with nanoparticles by the electrostatic deposition. The original micro-pin-fin surface was prepared by Professor Jinjia Wei's group (Xi'an Jiaotong University) who we collaborate with. It is seen that nanoparticles accumulated on the surface, especially on micro pin fins, forming structures randomly. It is expected that pool boiling performance is further enhanced by these nanoparticles.

Femtosecond laser technique

Figure 3.8 illustrates the working system of a femtosecond laser technique. In general, a femtosecond laser was used to get rid of some material on surfaces due to its high-density power, generating the designed surface morphology. In this thesis, a femtosecond laser (SpitfireAce-12FS) was selected to fabricate surfaces, while a processing station (LASER μFAB Newport) was used. The laser beam has a power of 2 W, and the processing station has an optical lens focal distance of 100 mm. During the fabrication, the laser beam scanning

velocity was controlled as 0.2 mm/s, and different laser beam power ratios were employed to generate structures with different size. An orthogonal scanning strategy was carried out to obtain micro pin fins on surfaces.

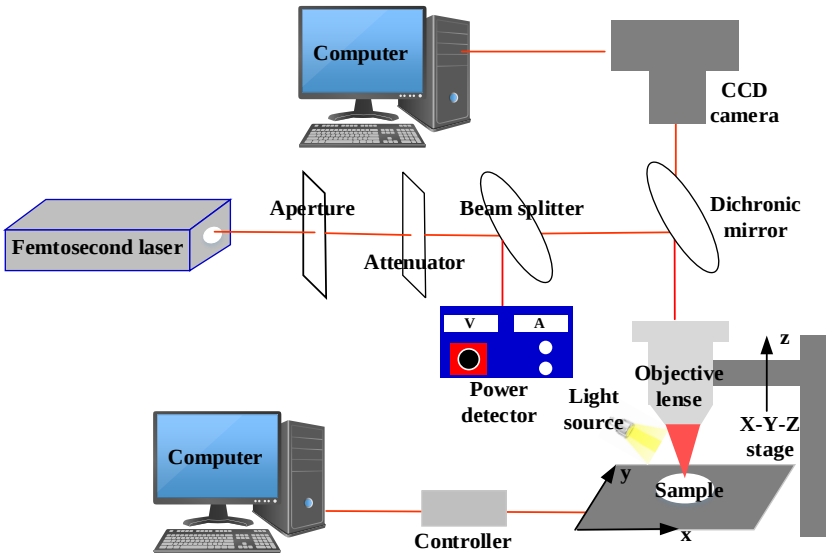

Figure 3.8: Schematic of the femtosecond laser process.

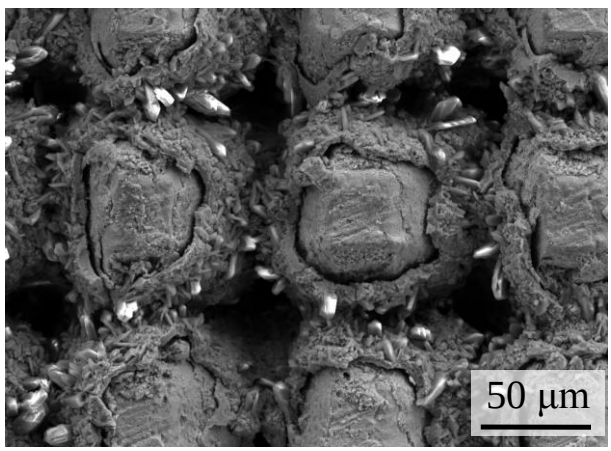

Figure 3.9: SEM images of a surface prepared by the femtosecond laser technique.

Figure 3.9 shows SEM images of a surface prepared by the femtosecond laser technique, with a 70% laser beam power ratio. It is obvious that micro pin fins are surrounded by a layer of porous structures which is composed of nanoparticles generated during the laser processing, and among micro pins are cavities. It is supposed that these cavities and rather rough surfaces of micro pin fins can increase active nucleation site density and enhance relevant wettability. Accordingly, pool boiling performance is expected to be augmented.

The SEM images were taken with a scanning electronic microscope (ZEISS, EVO LS 10) in Malmö University, and the roughness was measured with a 3D optical profiler (Dektak 6M) in NanoLund.

3.2 Test rigs

In this section, test rigs are introduced, including the facility to measure wettability (static contact angle, dynamic contact angle and wickability), and pool boiling facilities. This thesis involves saturated pool boiling on copper surfaces (85% tests) and subcooled pool boiling on silicon surfaces (15% tests). The facilities to measure wettability and study saturated pool boiling on copper surfaces were constructed in our group, while the facility to study subcooled pool boiling on silicon surfaces was available in Professor Jinjia Wei's group at Xi'an Jiaotong University, China.

Wettability measurement

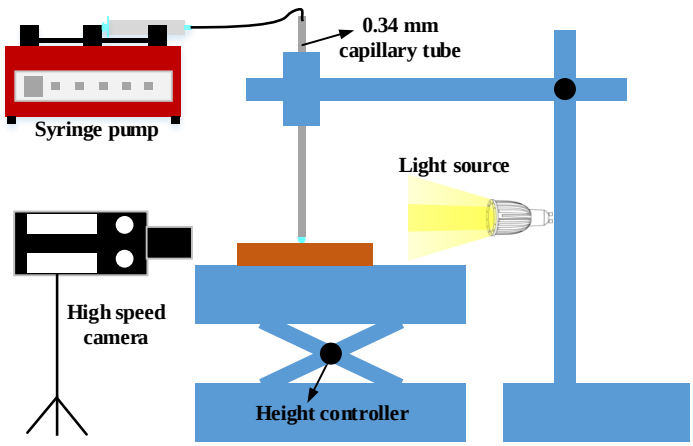

Figure 3.10: Schematic of the test rig to measure surface wettability.

Figure 3.10 indicates the setup to measure surface wettability. Contact angle is an important parameter to characterize the wettability, but it is not totally sufficient, especially for some well-wetting liquids (HFE-7200, NOVEC-649, FC-72, Pentane and Acetone in this thesis). Then, the wickability is measured through this setup, by comparing the spreading velocity of liquids on surfaces. In general, the setup mainly consists of a height controller to adjust the position of a platform where surfaces are placed, a glass micro capillary tube, a high-precision syringe pump (New Era, NE-400) and a high speed camera (Phantom v611).

To measure wickability of well-wetting liquids, the high speed camera was kept on, while the height controller was adjusted to let surfaces touch the mouth of the micro capillary tube where a volume of liquid was injected. Then, the liquid level in the capillary tube could be captured by the high speed camera with 1000 fps, and the liquid level dropping rate describes the surface wickablity.

Similarly, to measure static contact angles of well-wetting liquids, firstly a droplet was generated on the mouth of the capillary tube. Then, the high speed camera was on, and meanwhile the height controller was adjusted until the surface contacted with the droplet. The droplet revolution was recorded by the camera, which was divided into a spreading stage, a transitional stage and a steady stage, and the static contact angle was measured at the steady stage.

It is easier to measure the static contact angle of water. A water droplet of 10 µl was dropped on surfaces with a pipette, and then the droplet was recorded by the camera. To measure the dynamic contact angle of water, a syringe pump was used to exactly control the liquid rate (pumping or withdrawn). In this thesis, a water droplet of 10 µl was withdrawn at a rate of 0.5 µl/s, and droplet evolution was captured by the high speed camera with 100 fps to measure the receding contact angle.

Pool boiling test rigs

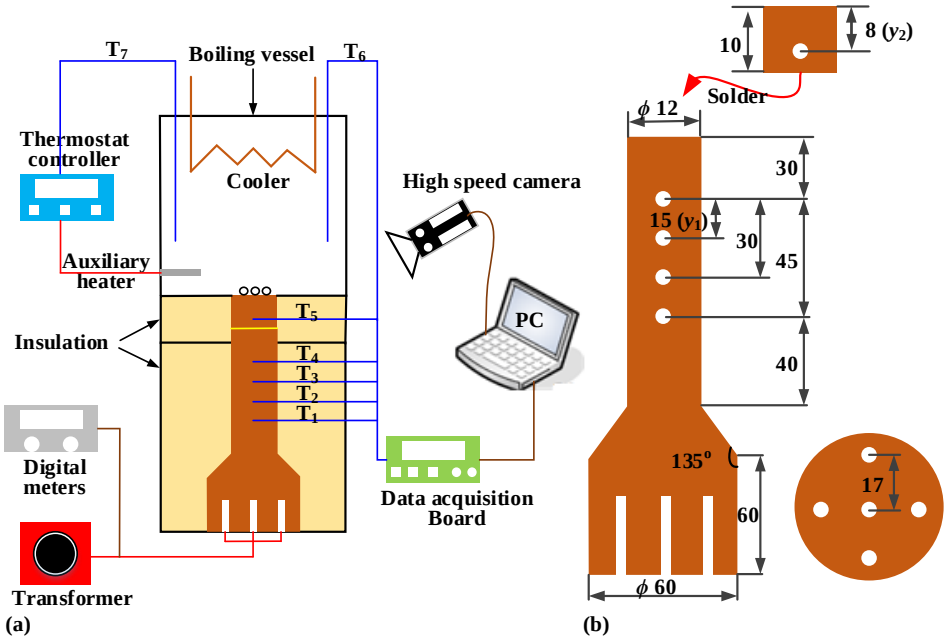

Figure 3.11: Schematic of the test rig of pool boiling on copper surfaces.

Figure 3.11(a) demonstrates the pool boiling test rig for copper surfaces. A copper rod was heated up with five cartridge heaters (CIR-10121, OMEGA) powered by a transformer (KIEA 8, Tufvassons Transformator) connected to two digital meters. A saturated state was achieved and kept with a temperature controller (MAXVU16), an auxiliary heater and a cooler. Temperatures were collected by a data acquisition board (Agilent 34970A) and bubble dynamics were recorded by a high speed camera (Phantom v611). Additionally, a vessel made of optic glass acted as the boiling chamber, which has a size of 100 mm × 100 mm × 300 mm

in length, width and height, respectively. The copper rod was covered with PTFE to minimize heat losses. A relief valve was mounted to guarantee an atmospheric surrounding during experiments.

Figure 3.11(b) shows details of the copper rod, i.e., the distribution of the thermocouples and cartridge heaters. Five cartridge heaters (CIR-10121 from OMEGA) were inserted into the bottom of the rod, with one in the center surrounded by the others symmetrically. The copper rod is a cylinder with a bottom diameter of 60 mm and a top diameter of 12 mm. At the height of 60 mm, the diameter of the rod transits smoothly from 60 mm to 12 mm with an angle of 135°. To evaluate the heat flux (q) and the boiling surface temperature (T_w), four K-type thermocouples were mounted on the rod vertically with 15 mm intervals and a K-type thermocouple was embedded in the test substrates at 8 mm from the boiling surface. The substrates had a height of 10 mm and a diameter of 12 mm. A tin paste (BERA-FIX soldering paste) was used to solder substrates onto the copper rod.

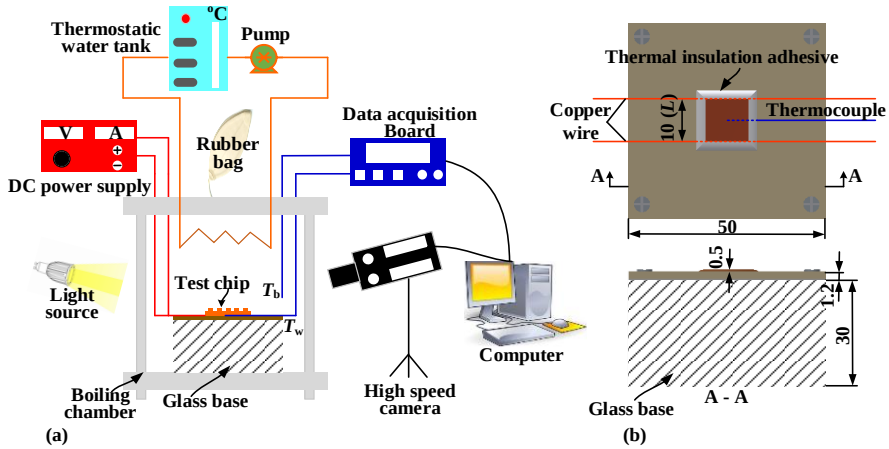

Figure 3.12: Schematic of the test rig of pool boiling on silicon surfaces.

Figure 3.12(a) illustrates the pool boiling test rig for silicon surfaces. A boiling chamber is made of polymethyl methacrylate with a size of 120 mm × 120 mm × 110 mm and a glass base of 50 mm × 50 mm × 30 mm was mounted inside the chamber to fix test surfaces which were Joule heated by a DC power supply (Agilent N5751A). A thermostatic water tank and an auxiliary heater were used to control the degree of subcooling. Wall and liquid temperatures were measured by T-type thermocouples. In addition, a rubber bag was connected with the boiling chamber to keep the pressure atmospheric. Temperatures were recorded by a data logger (DI710-UHS), and bubble behavior was captured by a high speed camera (VITcam CTC).

Figure 3.12(b) shows the details of the test section. A 10 mm (L) × 10 mm (L) × 0.5 mm (H) silicon surface was adopted in the experiment as the heater element. Two copper wires of 0.25 mm diameter were welded on two opposite edges of the test surface by an ultrasonic bonding method, avoiding a large contact resistance between the surface and the copper wires. A T-

type thermocouple of 0.13 mm diameter was adhered at the center of the back side of the test surface. The test surface was glued onto a thin polycarbonate plate of 50 mm × 50 mm × 1.2 mm by a thermal insulation adhesive which took 24 h to be effective. Then the thin polycarbonate plate was fixed on the glass base inside the boiling chamber.

3.3 Experimental procedure

Regarding saturated pool boiling on copper surfaces, about 1.0 liter of liquids was poured in the boiling vessel and vigorously boiled for half an hour to degas non-condensable gases. Voltage was increased by 3V and 5V for well-wetting liquids and water, respectively, case by case during experiments. The experiments ended when critical heat flux occurred. At the critical heat flux, an abrupt increase of temperature appeared. All data were collected at a steady state when the recorded temperatures deviated within ±0.2°C during 5 mins. The temperatures recorded during 2 mins were averaged as the final results. The experiments were repeated three times on each surface within 3 - 6 days.

Regarding subcooled pool boiling on silicon surfaces, the procedure was quite similar with that in experiments of the saturated pool boiling, except that experiments were carried out without degassing the liquid and voltage was increased by 2V each time, while a smaller step of 0.5V was adopted when the heat flux was close to the critical heat flux.

3.4 Data reduction and uncertainty analysis

Data reduction

In this thesis, copper surfaces were heated by conduction (**Papers** i-vi), while silicon surfaces were Joule heated (paper vii). Therefore, the heat flux calculation was different for the copper surfaces and the silicon surfaces.

For copper surfaces, the heat flux (q) was calculated by Fourier's law as

$$q = k_{\mathrm{Cu}} \frac{(T_1 - T_4)}{3y_1} \tag{3-2}$$

Accordingly, the copper surface temperature T_{w} was calculated as

$$T_{\mathrm{w}} = T_5 - \frac{q \times y_2}{k_{\mathrm{Cu}}} \tag{3-3}$$

where y_1 = 15 mm, y_2 = 8 mm and k_{Cu} = 400 W/(m·K) is the thermal conductivity of copper.

For silicon surfaces, the heat flux (q) was calculated by Joule's law as

$$q = \frac{U \cdot I}{A} = \frac{U \cdot I}{L \cdot L} \tag{3-4}$$

where L = 10 mm. The silicon surface temperature was directly measured by a thermocouple.

Then, heat transfer coefficient was calculated as

$$\mathrm{HTC} = \frac{q}{T_\mathrm{w} - T_\mathrm{l}} \tag{3-5}$$

T_l is the liquid temperature measured by a thermocouple.

Uncertainty analysis

Uncertainties were estimated using the method proposed by Moffat [81]. In general, according to Moffat, the uncertainty in the result F is a function of the independent variables X_i and is written as

$$F = F(X_\mathrm{i}) \tag{3-6}$$

The uncertainty of F is expressed as

$$\delta F = \left[\sum_{\mathrm{i}=1}^{\mathrm{n}} \left(\frac{\partial F}{\partial X_\mathrm{i}} \delta X_\mathrm{i}\right)^2\right]^{1/2} \tag{3-7}$$

where $\partial F/\partial X_\mathrm{i}$ and δX_i are the sensitivity coefficient and uncertainty level associated with the variable X_i, respectively. δX_i was obtained by a root-mean square combination of the precision uncertainty of the instruments and the unsteadiness uncertainty. $\partial F/\partial X_\mathrm{i}$ accounts for measurement resolution, instrumentation variance, geometric uncertainty, substrate conduction loss and calibration error. The variable X_i to be included in the calculation of the total uncertainty level of F depends on the purpose of the analysis. With this method, the uncertainties involved in this thesis are summarized in Table 3.1.

Table 3.1 Uncertainties.

Parameters	Uncertainty	Remarks
Thermocouple T	± 0.2 °C	-
Distance y_1, y_2	± 0.2 mm	-
Surface roughness Ra	± 2.0%	-
Contact angle	± 5.0 °	-
Copper surface temperature T_w	Max. ± 0.26 °C	$\delta T_\mathrm{w} = \left[(\delta T_5)^2 + \left(\frac{y_2}{k_\mathrm{Cu}}\delta q\right)^2 + \left(\frac{q}{k_\mathrm{Cu}}\delta y_2\right)^2\right]^{1/2}$
Superheat T_w-T_l	Max. ± 0.33 °C	$\delta(T_\mathrm{w} - T_\mathrm{l}) = [(\delta T_\mathrm{w})^2 + (\delta T_\mathrm{l})^2]^{1/2}$
Heat flux q	Max.± 11.4%	$\frac{\delta q}{q} = \left[\left(\frac{\delta T_4}{T_4 - T_1}\right)^2 + \left(\frac{\delta T_1}{T_4 - T_1}\right)^2 + \left(\frac{\delta y_1}{y_1}\right)^2\right]^{1/2}$

Heat transfer coefficient HTC	Max. ± 11.7%	$\frac{\delta \mathrm{HTC}}{\mathrm{HTC}} = \left[\left(\frac{\delta q}{q}\right)^2 + \left(\frac{\delta T_\mathrm{w}}{T_\mathrm{w} - T_\mathrm{l}}\right)^2 + \left(\frac{\delta T_\mathrm{l}}{T_\mathrm{w} - T_\mathrm{l}}\right)^2\right]^{1/2}$
Chord length of departure bubbles (a: chord length parallel to the surface; b: chord length perpendicular to the surface)	Max.± 22.1%	The departure bubbles have 4.8 to 20.0 pixels (x) in the direction parallel to the surface and 4.8 to 17.8 pixels (x') in the direction perpendicular to the surface, with a deviation of ± 1 pixel (δx, $\delta x'$). The length scales in parallel and perpendicular direction are 25 pixels (y) and 12.5 pixels (y') in 1 mm, respectively, with a deviation of ± 1 pixel (δy, $\delta y'$) $\frac{\delta a}{a} = \left[\left(\frac{\delta x}{x}\right)^2 + \left(\frac{\delta y}{y}\right)^2\right]^{1/2}$ $\frac{\delta b}{b} = \left[\left(\frac{\delta x'}{x'}\right)^2 + \left(\frac{\delta y'}{y'}\right)^2\right]^{1/2}$
Bubble departure diameter D_d	Max. ± 15.1%	$D_d = (a^2 b)^{1/3}$ $\frac{\delta D_\mathrm{d}}{D_\mathrm{d}} = \left[\left(\frac{2}{3}\frac{\delta a}{a}\right)^2 + \left(\frac{1}{3}\frac{\delta b}{b}\right)^2\right]^{1/2}$

Table 3.2 provides properties of the liquids that were tested in this thesis, including water, dielectric liquids (HFE-7200, NOVEC-649, FC-72) and organics liquids (pentane, acetone).

Table 3.2 Properties of liquids at saturated state.

	ρ_l kg/m^3	ρ_v kg/m^3	k_l W/(m·K)	μ_l mPa·s	C_pl J/(kg·K)	σ_lv mN/m	i_lv kJ/kg
water	958.4	0.60	0.677	0.282	4215.7	58.9	2256.4
HFE-7200	1303.0	10.30	0.056	0.348	1220.0	9.2	119.0
Novec-649	1513.0	13.42	0.059	0.450	1103.0	10.8	88.0
FC-72	1592.0	13.33	0.054	0.430	1101.0	7.9	76.9
Pentane	609.7	2.98	0.111	0.199	2367.5	14.2	357.6
Acetone	748.5	2.12	0.169	0.234	2276.9	19.1	520.6

CHAPTER 4

Results and Discussion

This chapter presents pool boiling results and related discussion. The prepared surfaces in each paper are introduced in the following, although probably not all results are shown and discussed in details to make the thesis readable. Some short names of the surfaces have been altered to suit the format of this thesis, compared with the names in papers.

Paper i: Nanoparticle coatings were prepared by the electrophoretic deposition method (EPD), with Cu-Zn nanoparticles. The details of the surfaces are indicated in Table 4.1.

Table 4.1 Test surfaces in paper i.

	Nanoparticles	Roughness	Static contact angle	Liquid
SS	-	0.109 μm	24.4°	
EPD-1	0.3mg Cu-Zn	0.541 μm	23.2°	
EPD-2	0.6mg Cu-Zn	0.550 μm	24.0°	HEE-7200
EPD-3	0.9mg Cu-Zn	1.276 μm	22.6°	
EPD-4	1.2mg Cu-Zn	1.435 μm	20.6°	

Paper ii: Modulated nanoparticle coatings were fabricated by the electrophoretic deposition method (EPD), with coexistence of smooth regions and coating regions, as shown in Figure 4.1. The details of the surfaces are shown in Table 4.2.

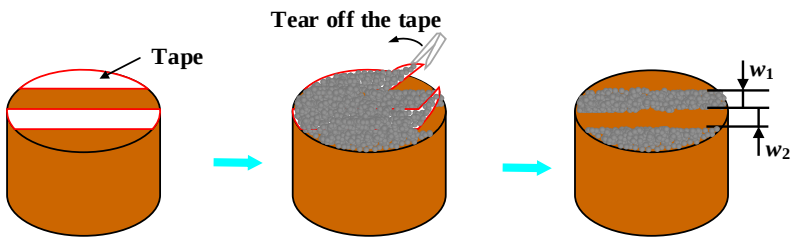

Figure 4.1: The fabrication of modulated nanoparticle coatings.

Table 4.2 Test surfaces in paper ii.

	Nanoparticles	w_1	w_2	Liquid
MEPD-1	0.6mg Cu-Zn	2 mm	2 mm	HEE-7200
MEPD-2	0.6mg Cu-Zn	3 mm	3 mm	
MEPD-3	1.2mg Cu-Zn	2 mm	2 mm	
MEPD-4	1.2mg Cu-Zn	3 mm	3 mm	

Note: MEPD-1, MEPD-2, MEPD-3 and MEPD-4 are MCS-1-1, MCS-1-2, MCS-2-1 and MCS-2-2, respectively, in paper ii.

Paper iii: Nanoparticle coatings and microporous coatings were prepared by the electrophoretic deposition method (EPD) and the electrochemical deposition method (ECD), respectively. The electrochemical deposition was carried out in an aqueous electrolyte solution, i.e., 0.4 M $CuSO_4$+1.5 M H_2SO_4 in water, with a current density of 1.0 A/cm^2 for various deposition durations. The surfaces are summarized in Table 4.3

Table 4.3 Test surfaces in paper iii.

	Nanoparticles	Roughness	Liquid
EPD-1*	0.98mg Cu	2.02 μm	HFE-7200 Acetone
EPD-2*	0.47mg Cu-Zn +0.51mg Cu	1.56 μm	
EPD-3*	1.5mg Cu	1.53 μm	
	Deposition time	Roughness	Liquid
ECD-1*	40s	2.34 μm	HFE-7200
ECD-2*	80s	1.92 μm	

Note: EPD-1*, EPD-2*, EPD-3*, ECD-1*and ECD-2*are EPD-1, EPD-2, EPD-3, ECD-1 and ECD-2, respectively, in paper iii.

Paper iv: Microporous coatings were prepared by the electrochemical deposition method (ECD). The electrochemical deposition was carried out in an aqueous electrolyte solution, i.e., various $CuSO_4$ concentration +1.5 M H_2SO_4 in water, with a current density of 1.0 A/cm^2 for 40 s. The surfaces are summarized in Table 4.4.

Table 4.4 Test surfaces in paper iv.

	$CuSO_4$ concentration	Roughness	Static contact angle	Liquid
ECD-1	0.1 M	10.99 μm	14.7°	NOVEC-649
ECD-2	0.2 M	14.24 μm	11.3°	
ECD-3	0.3 M	15.51 μm	10.2°	
ECD-4	0.4 M	17.00 μm	8.2°	

Note: ECD-1, ECD-2, ECD-3 and ECD-4 are ECDS-0.1M, ECDS-0.2M, ECDS-0.3M and ECDS-0.4M, respectively, in paper iv.

Paper v: Microporous coatings were prepared by the electrochemical deposition method (ECD). The aqueous electrolyte solution is the same as that in paper iii, i.e., 0.4 M $CuSO_4$+1.5

M H_2SO_4 in water. However, two types of deposition strategies were used. Three surfaces were reproduced by one-step deposition with a current density of 35 mA/cm^2 for 3600 s, and the other surface was prepared by two-step deposition with a current density of 1.0 A/cm^2 for 40 s, followed by a current density of 35 mA/cm^2 for 3600 s, as summarized in Table 4.5.

Table 4.5 Test surfaces in paper v.

	Deposition strategy	Static contact angle	Receding contact angle	Roughness	Liquid
SS	-	86.27°	64.04°	0.094 μm	Water
ECD-1s*	one-step	126.44°	82.09°	18.827 μm	
ECD-1s**	one-step	119.43°	29.21°	12.067 μm	
ECD-1s	one-step	117.58°	27.88°	3.548 μm	
ECD-2s	two-step	132.74°	68.20°	26.105 μm	

Paper vi: Nanoparticle coatings, micro pin fins and hybrid micro/nano structures were fabricated by the electrophoretic deposition (EPD), the femtosecond laser (FLS) and the composite method (FLS+EPD), respectively. The nanoparticle coating surface was the same as EPD-1* in Table 4.3. The femtosecond laser surfaces were labelled as FLS1 and FLS2, while the hybrid micro/nano surfaces were labelled as CS1 and CS2. Especially, the characterizations of FLS1 and FLS2 are shown in Table 4.6.

Table 4.6 Femtosecond laser surfaces in paper vi.

	Width of micro pin fins	Pitch of micro pin fins	Height of micro pin fins	Nanoparticles	Liquid
EPD-1*	-	-	-	0.98mg Cu	Pentane
FLS1	60.0 μm	100 μm	79.5 μm	-	
FLS2	107.5 μm	200 μm	157.0 μm	-	
CS1	60.0 μm	100 μm	79.5 μm	0.98mg Cu	
CS2	107.5 μm	200 μm	157.0 μm	0.98mg Cu	

Table 4.7 Tested surfaces in paper vii.

	Width of micro pin fins	Pitch of micro pin fins	Height of micro pin fins	Deposition time	Liquid
#1	30 μm	75 μm	60 μm	-	FC-72
#1-8h				8h	
#1-16h				16h	
#2	30 μm	60 μm	60 μm	-	
#2-8h				8h	
#2-16h				16h	

Paper vii: Hybrid micro/nano structures were prepared by depositing nanoparticles on micro-pin-fin silicon surface with the electrostatic deposition method (ESD). Table 4.7 summarizes the surfaces that were tested.

4.1 Validation of the test rig

Before moving onto the main results, it is essential to describe the validation of the experimental setup and procedure. For this purpose, pool boiling of DI water was tested on smooth copper surfaces. Because Vachon et al. [82] systematically evaluated constants for the Rohsenow pool-boiling correlation referring to a large amount of data on smooth surfaces, the constants for water on copper surfaces were recommend. The Rohsenow correlation can be expressed as [82]

$$q = \mu_l i_{lv} \left[\frac{g(\rho_l - \rho_v)}{\sigma_{lv}}\right]^{1/2} \left[\frac{c_{pl}(T_w - T_l)}{C_{sf} i_{lv} Pr_l^n}\right]^3 \quad (4\text{-}1)$$

where C_{sf} and n are the constants depending on the liquid-surface combination. As suggested by Vachon et al. [82], C_{sf} and n are 0.0154 and 1, respectively for water on copper surfaces.

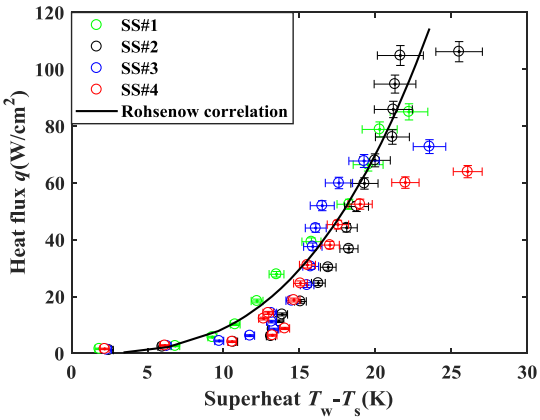

Figure 4.2: The comparison between the experimental results and the Rohsenow correlation, regarding pool boiling of water on smooth copper surfaces.

Pool boiling of water was tested on four smooth copper surfaces for repeatability. Figure 4.2 indicates the comparison between the experimental results and the Rohsenow correlation with the constants suggested by Vachon et al. [82]. It is evident that the experimental results are repeatable, and consistent with the results predicted by the Rohsenow correlation. Accordingly, the present test rig is deemed to be reliable.

4.2 Boiling curves

This section demonstrates pool boiling curves on the tested surfaces, including nanoparticle-coating surfaces, microporous surfaces, hybrid micro/nano-structure surfaces.

Nanoparticle-coating surfaces

Generally speaking, two types of nanoparticle-coating surfaces were prepared, which are homogeneous nanoparticle coatings and heterogeneous (modulated) nanoparticle coatings. On the homogeneous nanoparticle coatings, surfaces were completely covered with the

nanoparticles. However, on the heterogeneous coatings, coating regions and smooth regions coexisted on the surfaces. Pool boiling of HFE-7200 and acetone on these two types of surfaces was discussed in **Papers i, ii, iii**.

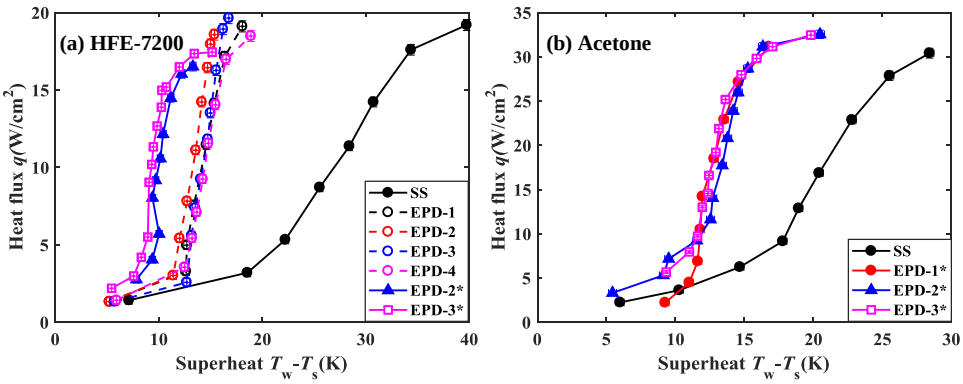

Figure 4.3: Pool boiling curves on homogeneous nanoparticle-coating surfaces: (a) HFE-7200, (b) Acetone.

Figure 4.3 shows pool boiling curves of HFE-7200 and acetone on the homogeneous nanoparticle-coating surfaces, indicating that the curves of nanoparticle-coating surfaces shift to the left, compared with that of a smooth surface (SS). EPD-1, EPD2-, EPD-3 and EPD-4 were deposited with Cu-Zn nanoparticles of different amount, while EPD-1* and EPD-3* were covered by Cu nanoparticles of different amount, and EPD-2* was modified by a mixture of Cu-Zn and Cu nanoparticles. By the comparison of EPD-1, EPD-2 and EPD-3 in Fig. 4.3(a) and EPD-1* and EPD-3* in Fig. 4.3(b), it is clear that the nanoparticle numbers slightly affect pool boiling performance. However, the nanoparticle properties can tailor the performance, e.g., the comparison of EPD-3 and EPD-3* in Fig. 4.3(a).

In summary, regarding well-wetting liquid, heat transfer coefficients are augmented considerably by the homogeneous coatings (a maximum 100% enhancement), probably because the coatings generate much more nucleation sites and modulate bubble dynamics. However, the critical heat flux is not improved. Therefore, it is essential to design coatings which can enhance the critical heat flux as well.

Inspired by the hydrodynamic instability mechanism of critical heat flux, proposed by Zuber [34], heterogeneous nanoparticle-coating surfaces were fabricated. It is supposed that the critical heat flux could be enhanced by tailoring the instability wavelength. Pool boiling of HFE-7200 was studied on the heterogeneous nanoparticle-coating surfaces which are summarized in Table 4.2. Figure 4.4 compares the boiling curves of heterogeneous coating surfaces and homogeneous coating surfaces. The results show that the critical heat flux is remarkably increased by the heterogeneous coatings, compared with that on a smooth surface, even though the heat transfer coefficients on the heterogeneous coating surfaces are a little lower than those on the homogeneous coating surfaces. For example, the critical heat fluxes

on SS, EPD-2 and MEPD-2 are 19.2 W/cm^2, 18.6 W/cm^2 and 25.7 W/cm^2, respectively, indicating an enhancement of around 35%.

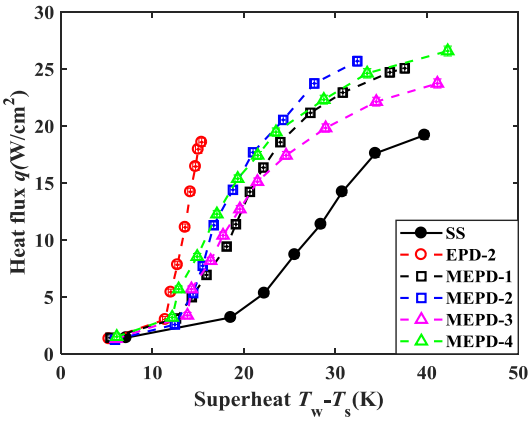

Figure 4.4: Pool boiling curves of HFE-7200 on heterogeneous nanoparticle-coating surfaces.

Microporous surfaces

In addition to the nanoparticle-coating surfaces discussed above, microporous coatings were deposited on copper surfaces by the electrochemical deposition method. Surfaces with different deposition time and $CuSO_4$ concentration were covered in **Paper iii** and **Paper iv**, respectively.

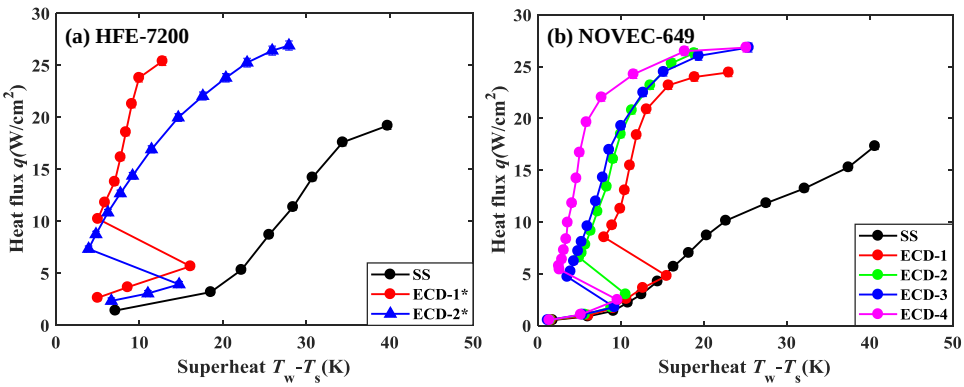

Figure 4.5: Pool boiling curves on microporous surfaces: (a) HFE-7200, (b) NOVEC-649.

Figure 4.5 indicates pool boiling curves of HFE-7200 and NOVEC-649 on microporous surfaces. It is found that heat transfer coefficients and critical heat flux are considerably enhanced by 230%-600% and 30-55%, respectively. However, a temperature excursion is detected on this type of surfaces. The occurrence of the temperature excursion is due to the surface characteristics and liquids. Regarding the microporous coatings in this thesis, there exist numerous micropores and microstructures of a size of tens to hundreds of micrometers,

which are readily wetted by well-wetting liquids, e.g., HFE-7200 and NOVEC-649. The well-wetted microstructures require a relatively high superheat to be activated. However, once they are activated, the vapor grows and spreads into other imperfections and serves as embryos to activate other sites. Therefore, the wall superheat suddenly drops. This temperature excursion was also detected in other studies, for example El-Genk and Ali [83] who studied pool boiling of PF-5060 on similar microporous surfaces.

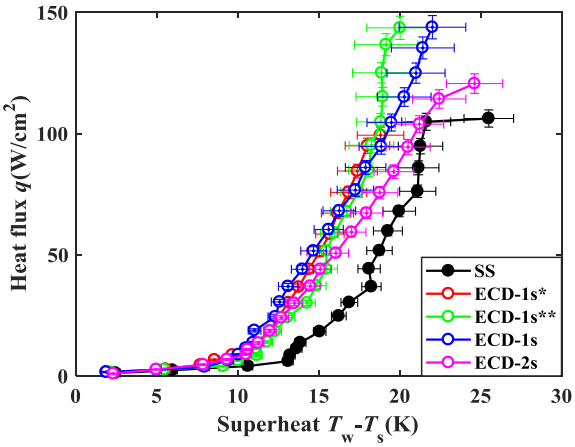

Figure 4.6: Pool boiling curves of DI-water on microporous surfaces.

In addition to the well-wetting liquids, pool boiling of water was also studied on microporous surfaces (**Paper v**). The microporous coatings in Fig. 4.5 were prepared by a large current density of 1.0 A/cm^2 for 10s - 40s, but these microporous coatings were not stable in water boiling. Then, three new microporous surfaces were produced at a very low current density of 35 mA/cm^2 for 3600s (ECD-1s, ECD-1s*, ECD-1s**) and another was prepared by two steps, first with 1.0 A/cm^2 for 40s and then 35 mA/cm^2 for 3600s (ECD-2s). It is found that these surfaces can be quite durable in water boiling. Figure 4.6 presents the pool boiling curves of water on these surfaces. It is seen that heat transfer is well repeated on ECD-1s, ECD-1s*and ECD-1s**, but ECD-1s* has a much lower critical heat flux than the others, which will be explained in a later section. Overall, heat transfer and critical heat flux both can be enhanced. A maximum enhancement of 56% can be achieved concerning heat transfer coefficients, while critical heat flux can be augmented by 13.6% - 35.4%. For example, the critical heat fluxes on SS and ECD-1s are 106.2 W/cm^2 and 143.9 W/cm^2, respectively.

Hybrid micro/nano-structure surfaces

Nanoparticle coatings and microporous coatings have been introduced above. The effect of hybrid micro/nano structures on pool boiling is discussed in this part. Two types of hybrid micro/nano structures were prepared. One type was fabricated on copper surfaces by a method combining the femtosecond laser technique and the electrophoretic deposition method (**Paper vi**). The other type was produced on silicon surfaces by a method combining the dry etching

and the electrostatic deposition method (**Paper vii**). Pool boiling of Pentane and FC-72 was tested in **Paper vi** and **Paper vii**, respectively.

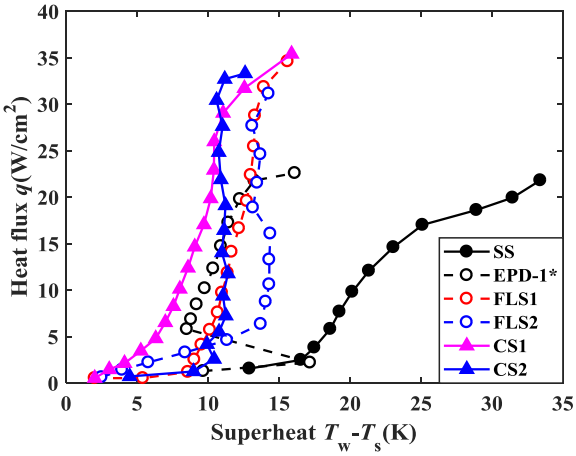

Figure 4.7: Comparison of pool boiling curves of Pentane on different surfaces.

Figure 4.7 compares pool boiling curves of Pentane on a smooth surface, a nanoparticle-coating surface, micro-pin-fin surfaces and hybrid micro/nano-structure surfaces. It is obvious that heat transfer is notably enhanced on these modified surfaces, compared with that on the smooth surface. However, the critical heat flux is still not enhanced by the nanoparticle coating, which further validates the observation in Fig. 4.3. Regarding the micro-pin-fin surfaces (FLS1 and FLS2), FLS2 behaves a little better than FLS1 at low and moderate heat fluxes, which is probably because of the different surface characteristics. Some nanowire-like structures were observed around the micro pin fins in the FLS2, which probably attribute to a larger amount of nucleation sites. In general, FLS1 and FLS2 have 60% - 100% higher heat transfer coefficients than the smooth surface. Concerning the critical heat flux, FLS1 and FLS2 have 46% - 59% higher values than the smooth surface. However, the hybrid micro/nano-structure surfaces (CS1 and CS2) perform the best among these surfaces. The heat transfer coefficients are further enhanced by 15% - 33%, in comparison to the micro-pin-fin surfaces, though the critical heat flux changes slightly.

Different from the studies above, subcooled pool boiling of FC-72 was investigated on silicon surfaces (**Paper vii**), including a smooth silicon surface, micro-pin-fin surfaces and hybrid micro/nano-structure surfaces. Figure 4.8 shows the boiling curves of FC-72 on these silicon surfaces at three subcoolings. Overall, heat transfer and critical heat flux are improved by micro pin fins and hybrid micro/nano structures. The further effect of nanoparticle coatings on the heat transfer depends on the layout of the micro pin fins on surfaces. For example, the surfaces #1-8h and #1-16h have significantly better heat transfer performance than the surface #1 on which the micro pin fins lay in a staggered way. However, the surfaces #2-8h and #2-16h have slightly different heat transfer performance from the surface #2 on which the micro pin fins lay in an aligned way. Concerning the critical heat flux, the hybrid micro/nano-

structure surfaces (#1-8h, #1-16h, #2-8h and #2-16h) have roughly higher values than the micro-pin-fin surfaces (#1 and #2), which is attributed to the further enhancement of liquid wickablity.

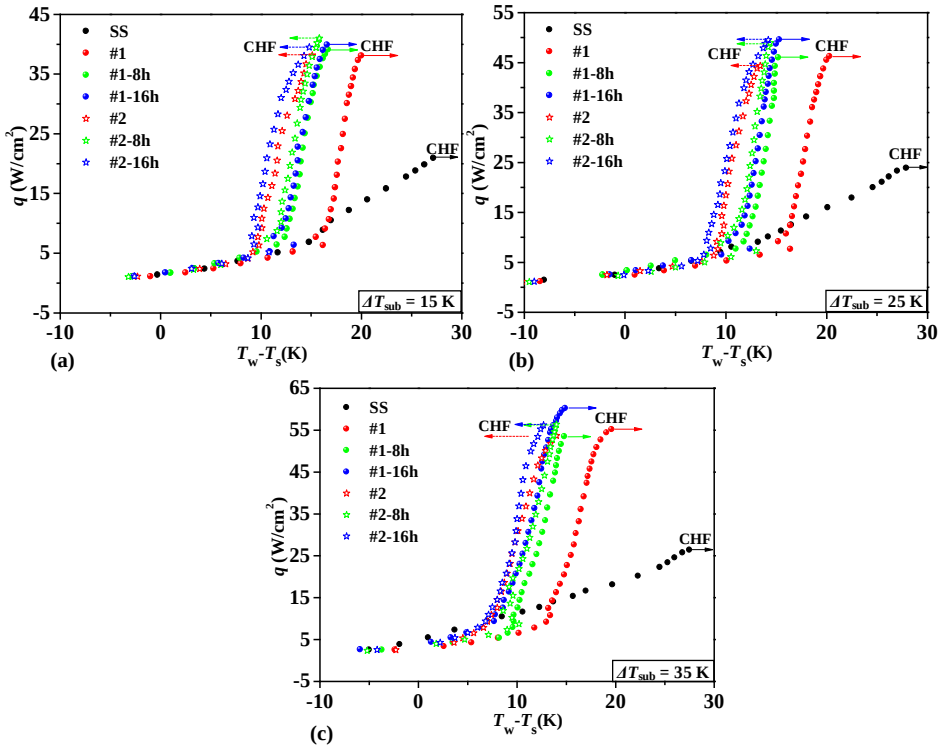

Figure 4.8: Comparison of pool boiling curves of FC-72 on different surfaces.

4.3 Bubble dynamics

In this section, bubble nucleation, bubble departure diameter and bubble departure frequency are elaborated. For this purpose, the relevant study of water is firstly presented, because water has a larger departure diameter and a smaller departure frequency, compared with the well-wetting liquids, and accordingly clear isolated bubbles can be detected in the boiling of water, while tens and hundreds of bubbles appear in the boiling of the well-wetting liquid, making it difficult to detect an individual bubble cycle. Then, averaged bubble departure diameters of the well-wetting liquids are shown at the end.

Single bubble nucleation

Single bubble nucleation has been studied in many investigations, e.g., Siedel et al. [84], Nam et al. [85], Jo et al. [86], Shen et al. [87] and Allred et al. [88]. Figure 4.9 compares the bubble growth dynamics of water (**Paper v**) on the smooth surface (SS) and the microporous surface (ECD-1s). It is obvious that the bubble on the SS has a longer growth cycle and a larger

departure diameter than those on the ECD-1s. In general, a bubble growth cycle can be sorted as two regions: the inertia-controlled region and the thermal-controlled region. The bubble grows quickly in the inertia-controlled region and grows slightly in the thermal-controlled region. For simplicity, the bubble can be assumed to be controlled by a buoyancy force and a surface tension force. The buoyancy force lifts the bubble, while the surface tension force holds the bubble. By playing the high speed video, it is found that the bubble on the SS has a large base area at the initial growth stage (like from 0 ms to 17 ms in Fig. 4.9(a)), and afterwards, the base area shrinks with time (like from 17 ms to 22 ms in Fig. 4.9(b)). However, the bubble on the ECD-1s always has a small base area and the base area is kept almost the same in the growth cycle (like from 0 ms to 11 ms in Fig. 4.9(b)), or at least the shrinking behavior is not apparently detected. The large base area provides a large surface tension force. Therefore, the bubble should grow larger to obtain a larger buoyancy force until departure. As a result, the SS has a larger bubble departure diameter and a longer departure time.

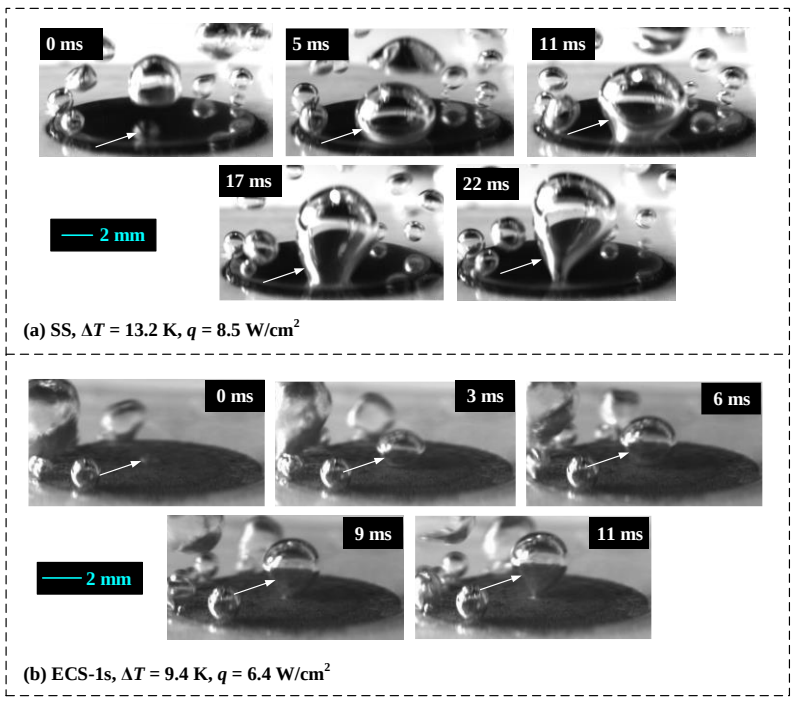

Figure 4.9: Bubble growth dynamics and ebullition cycle.

Bubble departure diameter and frequency

Bubble departure diameters and frequencies of water were quantitatively measured from high speed videos. The bubble departure diameter was averaged for 10 isolated bubbles, while the bubble departure frequency was obtained by accounting the total time of 10 bubbles. Figure 4.10 compares the bubble departure diameter and frequency on the smooth surface and microporous surfaces. It is obvious that bubbles on the microporous surface have smaller

departure diameter and higher departure frequency. These facts provide a direct explanation why the microporous surface has a better heat transfer performance.

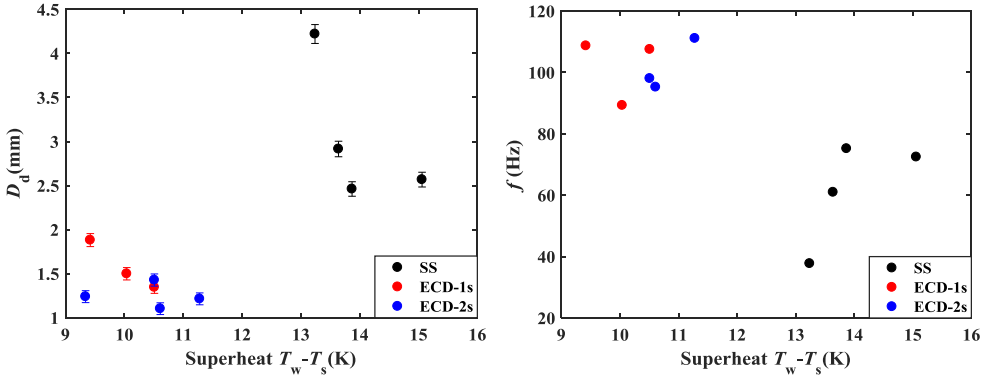

Figure 4.10: Bubble departure diameter and frequency against superheat in water boiling

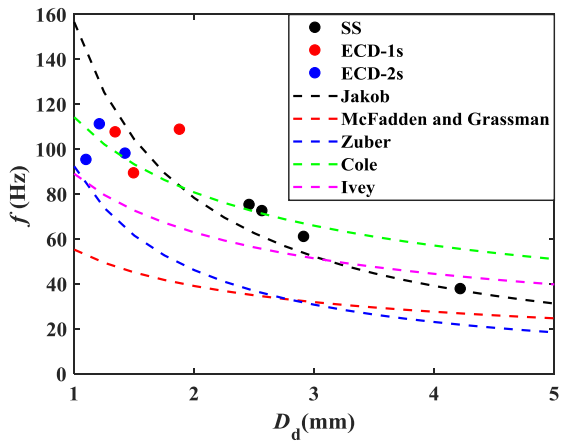

Figure 4.11: Relationship between bubble departure diameter and frequency in water boiling.

Regarding the relationship between bubble departure diameters and frequencies, extensive studies have been carried out, which are reviewed by Mohanty and Das [33]. A few of them are summarized in Table 4.8, and are compared with the present experimental data in Fig. 4.11. This figure illustrates that the present results coincide with the study by Jakob [89]. The present study further validates that smaller departure diameters induce faster releasing, which is preferable for boiling heat transfer.

Table 4.8 a few relationships between bubble departure diameter and frequency

Authors	Relationship
Jakob [89]	$fD_{\mathrm{d}} = \left[\frac{\sigma_{\mathrm{lv}} g(\rho_{\mathrm{l}} - \rho_{\mathrm{v}})}{\rho_{\mathrm{l}}^2}\right]^{1/4}$
McFadden and Grassman [90]	$fD_{\mathrm{d}}^{0.5} = 1.75$
Zuber [91]	$fD_{\mathrm{d}} = \left(\frac{1.18}{2}\right)\left[\frac{\sigma_{\mathrm{lv}} g(\rho_{\mathrm{l}} - \rho_{\mathrm{v}})}{\rho_{\mathrm{l}}^2}\right]^{1/4}$
Cole [92]	$fD_{\mathrm{d}}^{0.5} = \left[\frac{4g(\rho_{\mathrm{l}} - \rho_{\mathrm{v}})}{3\rho_{\mathrm{l}}}\right]^{1/4}$
Ivey [93]	$fD_{\mathrm{d}}^{0.5} = 0.9g^{1/2}$

In addition to bubble dynamics of water, bubble departure diameters of well-wetting liquids were also measured. However, it is difficult to detect bubble departure frequencies of well-wetting liquids in experiments, because the number of bubbles on surfaces is huge and it is nearly impossible to monitor a specific bubble in the whole cycle. In this case, a reliable relationship between bubble departure diameter and frequency can be employed to evaluate the bubble departure frequency.

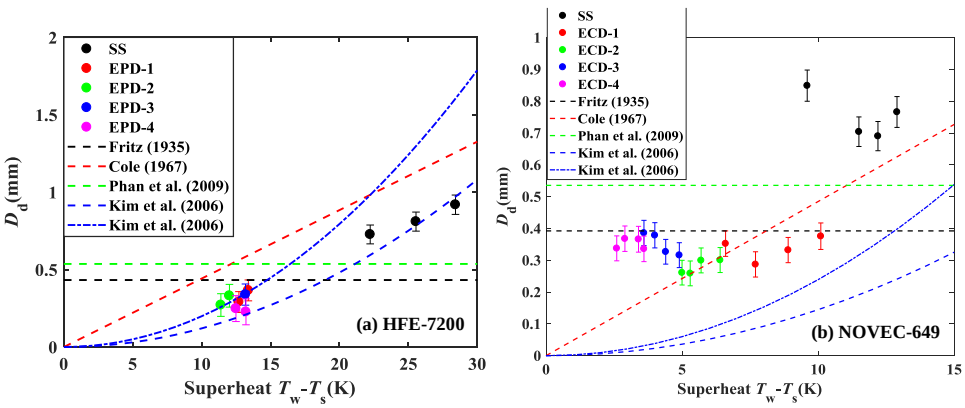

Figure 4.11: Comparison of bubble departure diameters with models: (a) **Paper i:** HFE-7200, (b) **Paper iii:** NOVEC-649.

Figure 4.11(a) and (b) present bubble departure diameters of HFE-7200 and NOVEC-649 against superheats, respectively, which are compared with several models, i.e., Fritz [94], Cole [92], Phan et al. [95], Kim et al. [96]. The formulas of these models can be found in **Paper i**. Overall, the modified surfaces have smaller bubble departure diameters than the smooth surface, and it is obvious that some models can predict the present results, to some extent. For example, regarding HFE-7200 boiling on the nanoparticle-coating surfaces (EPD), as shown in Fig. 4.11(a), the bubble departure diameters can generally be predicted by the model proposed by Kim et al. [96], while concerning NOVEC-649 boiling on the microporous surfaces (ECD), as shown in Fig. 4.11(b), the bubble departure diameters can roughly be

predicted by the model proposed by Fritz et al. [94]. Accordingly, the bubble departure frequency of HFE-7200 and NOVEC-649 is supposed to be evaluated by the corresponding models.

In summary, this section describes bubble dynamics quantitatively, including single bubble nucleation, bubble departure diameter and bubble departure frequency. Especially, the relationship between the bubble departure diameters and frequencies of water is validated by correlations in the literature, while the bubble departure diameters of the well-wetting liquids are compared with available models to find the approximate relationship which can evaluate the corresponding departure frequencies. In fact, information of bubble departure diameters and bubble departure frequencies are essential for the mechanistic heat transfer modelling presented in the following section.

4.4 Analysis of heat transfer

This section attempts to analyze heat transfer performance mechanistically and empirically. As introduced in section 2.2, the nucleate boiling heat transfer is possibly attributed to the natural convection, the transient conduction, the microlayer evaporation and the transient micro convection. Generally, it is assumed that the natural convection occurs in a bubble-uninfluenced area, while the others account for a bubble-influence area. The uninfluenced area is the area of a diameter larger than twice the bubble departure diameters, while the influenced area is the area of a diameter twice the bubble departure diameters, suggested by Mikic and Rohsenow [18].

In this thesis, a mechanistic heat transfer model was first constructed by considering the natural convection, the transient conduction and microlayer evaporation. The transient conduction model proposed by Mikic and Rohsenow [18] was employed in the present model. More details about the model constructions are elaborated in **Paper i** and **Paper ii**. The formula is expressed as

$$q = q_{\mathrm{nc}} + q_{\mathrm{cond}} + q_{\mathrm{me}} = 0.14\rho_{\mathrm{l}}C_{\mathrm{pl}}\left[\frac{\beta g(T_{\mathrm{w}}-T_{\mathrm{s}})^4\alpha_{\mathrm{l}}^2}{\nu_{\mathrm{l}}}\right]^{\frac{1}{3}}(1 - Na\cdot\pi D_{\mathrm{d}}^2) + 2\sqrt{\pi}\sqrt{(\rho k C_{\mathrm{p}})_{\mathrm{l}}}\sqrt{f}D_{\mathrm{d}}^2(T_{\mathrm{w}}-T_{\mathrm{s}})\cdot Na + \frac{2\pi}{3}\left(\frac{D_{\mathrm{d}}}{2}\right)^3\rho_{\mathrm{v}}i_{\mathrm{lv}}f\cdot Na \quad (4\text{-}2)$$

where, α_{l}, β and ν_{l} are liquid thermal diffusivity, liquid thermal expansion coefficient and liquid kinematic viscosity, respectively. Na is the active nucleation site density.

Equation (4-2) indicates that it is essential to obtain bubble departure diameters, bubble departure frequencies and active nucleation site densities to mechanistically model the heat transfer. The bubble departure diameters and frequencies have been discussed in the last section, while the active nucleation site density is unknown. It will be good if the active nucleation site density can be evaluated through the high speed video. However, it is quite difficult to count the number of bubbles on surfaces, especially for the well-wetting liquids. Therefore, the active nucleation site density is evaluated by suitable correlations in this thesis.

Regarding the smooth surface, it is found that the correlation proposed by Benjamin and Balakrishnan [19] is suitable, which is expressed as

$$Na_{\text{smooth}} = 218\text{Pr}^{1.63}\left(\frac{k_{\text{l}}\cdot\rho_{\text{l}}\cdot c_{\text{pl}}}{k_{\text{cu}}\cdot\rho_{\text{cu}}\cdot c_{\text{pcu}}}\right)\Psi^{-0.4}(T_{\text{w}}-T_{\text{s}})^3 \tag{4-3}$$

$$\Psi = 14.4 - 4.5\left(\frac{RaP_{\text{l}}}{\sigma_{\text{lv}}}\right) + 0.4\left(\frac{RaP_{\text{l}}}{\sigma_{\text{lv}}}\right)^2 \tag{4-4}$$

where, P_{l} is the liquid pressure, and Ra is the roughness.

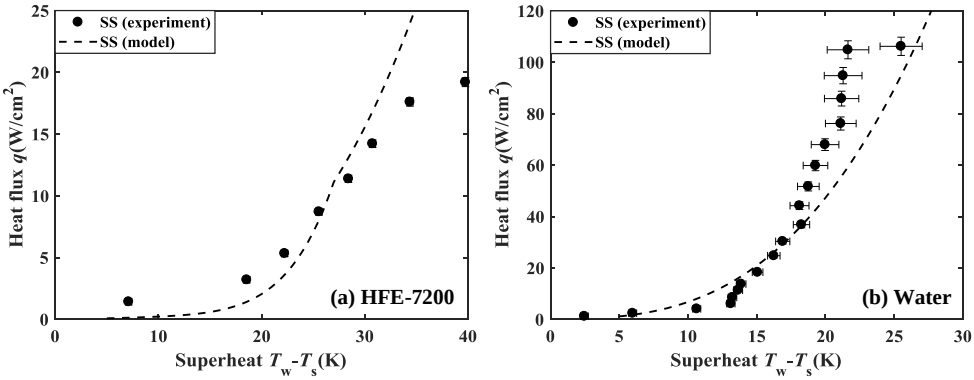

Figure 4.12: Comparison of boiling curves on smooth surfaces between experiments and models: (a) **Paper i:** HFE-7200, (b) **Paper v:** Water.

Right now, all information is available to model the heat transfer on smooth surfaces. Figure 4.12 illustrates the comparison of boiling curves of HFE-7200 and water on smooth surfaces between experiments and models. It is seen that the model can generally predict the boiling curves no matter for the well-wetting liquid or for water. Especially, the prediction is good at low heat fluxes, i.e., q < 10 W/cm^2 for HFE-7200 and q < 40 W/cm^2 for water. When the heat flux increases, bubble interactions become intensive, which probably affect the final heat transfer performance, but the proposed model does not consider the bubble interactions.

Regarding the modified surfaces, it is not suitable to use Equation (4-3) to estimate the active nucleation site density, because the equation indicates that the active nucleation site density decreases with increasing roughness, which is not consistent with the reality. Therefore, additional efforts are required to find other alternatives for the modified surfaces, e.g., nanoparticle-coating surfaces and microporous surfaces. Kocamustafaogullari and Ishii [97], Wang and Dhir [98], Basu et al.[99], and Hibiki and Ishii [100] also studied active nucleation site densities. Especially Wang and Dhir [98], Basu et al. [99], and Hibiki and Ishii [100] considered the effect of surface contact angles, and gave corresponding correlations which were suggested for cases where the contact angle is smaller than 90°.

In this thesis, surface wettability is supposed to be tailored by the coatings, to some extent, and the well-wetting liquids have contact angles smaller than 90°. Accordingly, regarding the well-wetting liquid on the coating surfaces, the active nucleation site density is evaluated by

the Hibiki - Ishii correlation [100] which has been stated to be suitable for well-wetting liquids in the literature, e.g., Thiagarajan et al. [101].

$$Na_{\text{coating}} = N\left\{1-\exp\left(-\frac{\theta^2}{8\theta'^2}\right)\right\}\left[\exp\left\{f(\rho^+)\frac{\lambda'}{L}\right\}-1\right] \tag{4-5}$$

$$L = \frac{2\sigma[1+(\rho_{\text{v}}/\rho_{\text{l}})]P_l}{\exp[i_{\text{lv}}(T_{\text{w}}-T_{\text{s}})/(RT_{\text{w}}T_{\text{s}})]-1} \tag{4-6}$$

$$f(\rho^+) = -0.01064 + 0.48246\rho^+ - 0.22712(\rho^+)^2 + 0.05468(\rho^+)^3 \tag{4-7}$$

$$\rho^+ = \log\left(\frac{\rho_{\text{l}}-\rho_{\text{v}}}{\rho_{\text{v}}}\right) \tag{4-8}$$

where, θ' and λ' are equal to 0.722 rad and 2.50×10^{-6} m, respectively. R is the gas constant. N is the average site density suggested as $5\times4.72\times10^5$. P_{l} is the liquid pressure which is the atmospheric pressure.

However, regarding water on the coating surfaces, the contact angle is much larger than 90°. Then, the correlations above might not be suitable. In this case, a new correlation is proposed based on bubble departure diameters. Assuming that a surface is completely uniformly covered with bubbles, then the number of bubbles is inversely proportional to the square of bubble departure diameters. As a consequence, the active nucleation density on the coating surface can be estimated by that on the smooth surface, with a formula as follows

$$Na_{\text{coating}} = \left(\frac{D_{\text{d,coating}}}{D_{\text{d,SS}}}\right)^2 Na_{\text{SS}} \tag{4-9}$$

where $(D_{\text{d,coating}}/D_{\text{d,SS}})^2$ is recommended as 4.5 - 6.0, based on the results in Fig. 4.10. Na_{SS} is obtained from the Equation (4-3). Referring to the analysis above, heat transfer of HFE-7200 and water on the coating surfaces can be modeled as well.

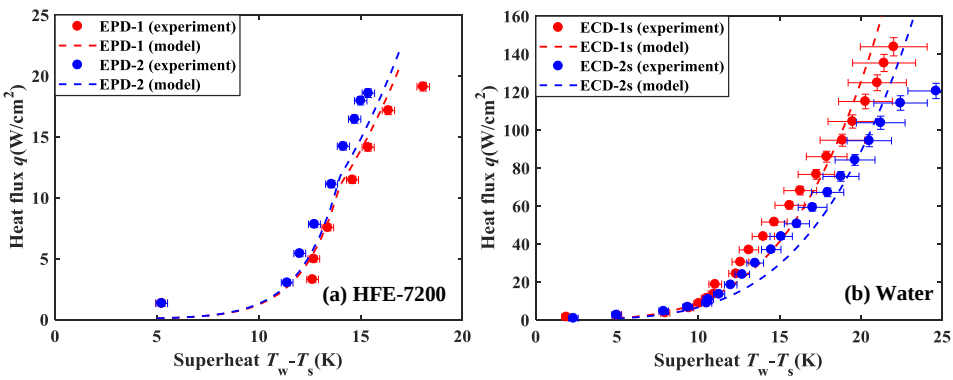

Figure 4.13: Boiling curves of experiments and models: (a) HFE-7200 on nanoparticle-coating surfaces (**Paper i**), (b) water on microporous surfaces (**Paper v**).

Figure 4.13 shows the predicted and experimental boiling curves, concerning HFE-7200 on the nanoparticle-coating surfaces and water on microporous surfaces. It is evident that the model can predict the heat transfer on the coating surfaces, to some extent.

It should be kept in mind that the model above does not consider the transient micro convection. However, it has been found numerically, e.g., Nam et al. [85], that in a bubble cycle, eddies exist in the liquid around bubbles. Especially, Haider and Webb [25] emphasized that eddies at bubble departure impose front and inverted stagnation liquid flows, intensifying an unsteady laminar forced-convection heat transfer from the nucleation sites. Referring to Haider and Webb [25], another model was proposed in **Paper iii** to predict the heat transfer on coating surfaces. This model considers the transient conduction, the transient micro convection and the microlayer evaporation, but neglects the natural convection which is found negligible. It is supposed that for a bubble cycle, the initial stage of bubble growth is dominated by the transient conduction, while the final stage of bubble growth and waiting time are dominated by the transient micro convection. These two parts are matched by an asymptotic expression proposed in [25], and the final expression is shown as follows

$$q_{\mathrm{cond}} + q_{\mathrm{mc}} + q_{\mathrm{me}} = 2\sqrt{\pi \cdot f \cdot k_{\mathrm{l}} \cdot \rho_{\mathrm{l}} \cdot C_{\mathrm{pl}}}\, D_{\mathrm{d}}^2 (T_{\mathrm{w}} - T_{\mathrm{s}}) \left[1 + \left(\frac{0.66\pi c}{\mathrm{Pr}_{\mathrm{l}}^{1/6}}\right)^m\right]^{\frac{1}{m}} \cdot Na + \frac{2\pi}{3}\left(\frac{D_{\mathrm{d}}}{2}\right)^3 \rho_{\mathrm{v}} i_{\mathrm{lv}} f \cdot Na \quad (4\text{-}10)$$

where c quantifies the strength of the stagnation flow and m is an asymptotic power index.

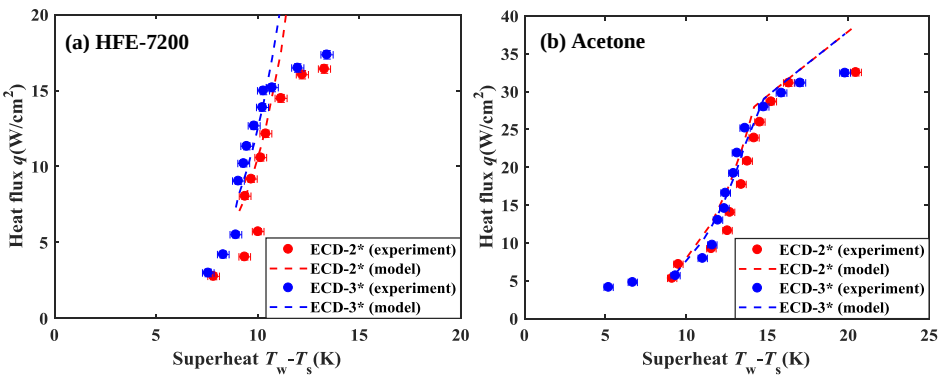

Figure 4.14: Boiling curves on nanoparticle-coating surfaces of experiments and models (**Paper iii**).

Figure 4.14 compares the boiling curves of experiments and models (Eq. (4-10)) for HFE-7200 and Acetone on nanoparticle-coating surfaces. It is evident that the proposed model can predict the experimental data relatively well, especially at relatively low to moderate heat fluxes.

In addition to the mechanistic heat transfer models above, several correlations were also compared with the experimental results in **Paper iv** which considered pool boiling of NOVEC-649 on microporous surfaces. The expressions of the correlations can be found in **Paper iv**. Figure 4.15 shows the comparison between experiments and correlations. It is seen that the heat transfer coefficient (HTC) is roughly consistent with some correlations, for

example the Cooper correlation [28] and the Rohsenow correlation [82] for smooth surfaces. However, it is difficult to predict the heat transfer on the microporous surfaces with a specific correlation.

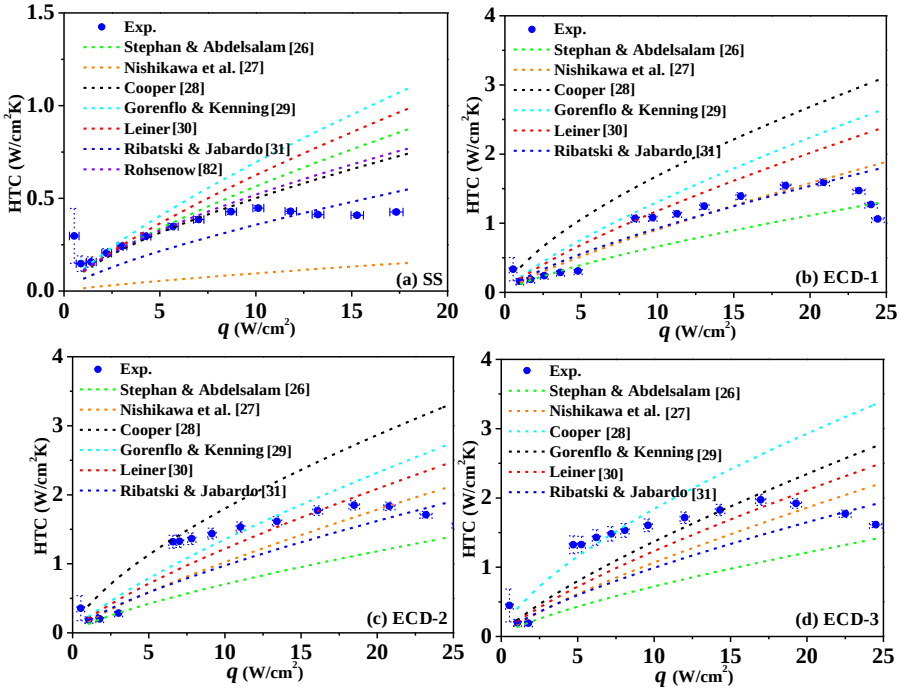

Figure 4.15: Comparisons between experiments and correlations, concerning heat transfer coefficient (HTC).

In summary, this section discussed heat transfer prediction with mechanistic models and empirical correlations. Two mechanistic models were constructed, referring to pioneering studies, which showed good predictions. Several typical correlations were compared, exploring their potential to predict the heat transfer on modified surfaces.

4.5 Analysis of critical heat flux

In this section, critical heat fluxes are analyzed with suitable mechanisms. The critical heat flux mechanisms have been briefly reviewed in the section 2.3, including the hydrodynamic instability model by Zuber [34], the macrolayer dry-out model by Haramura and Kattto [35], the hot/dry spot model by Yagov [36], the lift-off model by Guan et al. [39] and the force balance model by Kandlikar [40]. With the progress of boiling, these models have been extended to non-smooth surfaces. For example, Chu et al. [42] modified the Kandlikar model, considering the effect of roughness factor, while Quan et al. [43] added a wicking force in the Kandlikar model. Rahman et al. [41] and Ahn et al. [102] added an item into the Zuber model and the Kandlikar model, respectively, considering the contribution of wickability.

In this thesis, the wickability was measured with a micro capillary tube, which characterize the ability of liquid supplement. Figure 4.16 shows an example how the wickabiltiy was measured for NOVEC-649 on a smooth surface. The liquid level in the micro capillary tube is captured by a high speed camera, and then the volume absorbed by the surface can be obtained by multiplying the liquid drop height (h) by the wetting area (A_w).

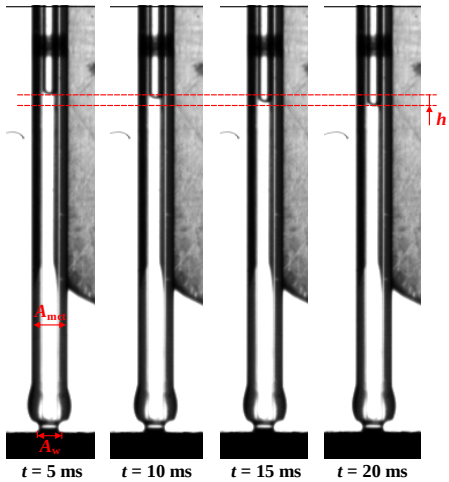

Figure 4.16: Visualization of wickability of NOVEC-649 on a smooth surface.

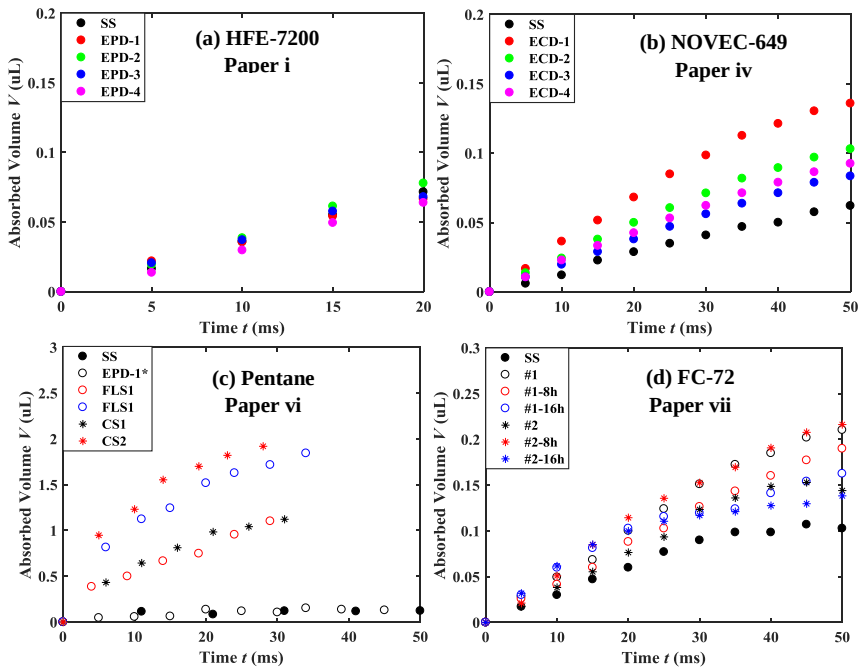

Figure 4.17: Experimental measurement of wickability on different surfaces.

Figure 4.17(a-d) compares the wickability on the nanoparticle-coating copper surfaces, the microporous copper surfaces, the hybrid micro/nano-structure copper surfaces and the hybrid micro/nano-structure silicon surfaces, respectively. It is shown that the wickabiltiy is not enhanced remarkably on the nanoparticle-coating surfaces, compared with the smooth surface, while the wickabiltiy is considerably enhanced on the other surfaces. This provides a good explanation why the critical heat flux is not improved by the nanoparticle coatings, but is improved by other surfaces.

Referring to Rahman et al. [41] and Ahn et al. [102], a critical heat flux (CHF) correlation is proposed, considering the contribution of wickability and subcooling. The item related to subcooling is zero in the saturated case. The formula is shown below

$$\mathrm{CHF} = \mathrm{CHF}_{\mathrm{SS}} + k_1 \frac{\rho_l i_{lv} d(V - V_{\mathrm{SS}})}{A_w dt} + k_2 \Delta T_{\mathrm{sub}} \tag{4-11}$$

where the coefficients k_1 and k_2 depends on the combination of liquids and surfaces. For example, Rahman et al. [41] suggested k_1 = 0.131 for water on silicon surfaces. However, k_1 and k_2 are suggested as 0.189 and 0.678 in the subcooled boiling of FC-72 on silicon surfaces (**Paper vii**), while for the saturated boiling of HFE-7200, NOVEC-649 and Pentane in Papers iii, iv and vi, respectively, k_1 = 0.131(**Papers iii, iv)** and 1.48 (**Papers vi)** are recommended.

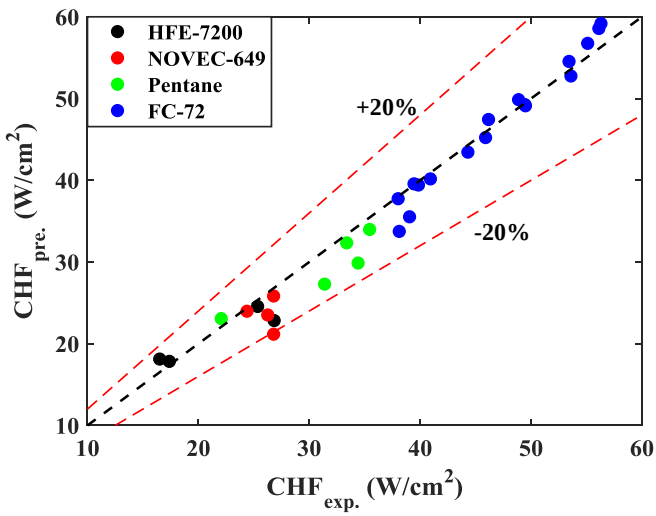

Figure 4.18: Comparison of predicted CHFs and experimental CHFs, considering wickablity.

Figure 4.18 compares the CHFs predicted by Eq. (4-11) and experimental CHFs. It is seen that the CHFs can be predicted well with a deviation ±20%, by considering the enhancement due to the wickability.

However, regarding the boiling of water in **Paper v**, the wickability cannot be measured by this method, because the microporous surfaces show hydrophobic characteristics for water.

Therefore, the critical heat flux of water cannot be related to the wickability, and some other mechanisms need to be clarified. In the study of water boiling, four microporous surfaces were prepared, i.e., ECD-2S, ECD-1s, ECD-1s* and ECD-1s**. The results show that the critical heat flux is enhanced on ECD-2S, ECD-1s and ECD-1s**, but deteriorates slightly on ECD-1s*. It is found that static contact angles on ECD-2S, ECD-1s, ECD-1s* and ECD-1s** are larger than that on the smooth surface (SS), but the receding contact angles decrease considerably on ECD-2S, ECD-1s and ECD-1s**, and increase slightly on ECD-1s*. For example, the static contact angles were measured as 86.27°, 126.44° and 119.43° on SS, ECD-1s* and ECD-1s**, respectively, while the receding contact angles were measured to be 64.04°, 82.09° and 29.21° on SS, ECD-1s* and ECD-1s**, respectively. Accordingly, the critical heat flux of water on copper surfaces is probably dependent on the receding contact angle. Kandlikar [40] proposed a critical heat flux mechanism, considering a momentum force, two surface tension forces and a hydrostatic head force, and assumed that the critical heat flux occurs when these forces reach a balanced state, driving bubbles to spread on the surfaces. Especially, in this model, the receding contact angle is an essential parameter, as follows

$$\mathrm{CHF} = i_{\mathrm{lv}}\rho_{\mathrm{v}}^{1/2} \cdot [\sigma(\rho_{\mathrm{l}} - \rho_{\mathrm{v}})g]^{1/4} \cdot \frac{1+\cos\theta_{\mathrm{rec}}}{16} \cdot [\frac{2}{\pi} + \frac{\pi}{4}(1+\cos\theta_{\mathrm{rec}})]^{1/2} \quad (4\text{-}12)$$

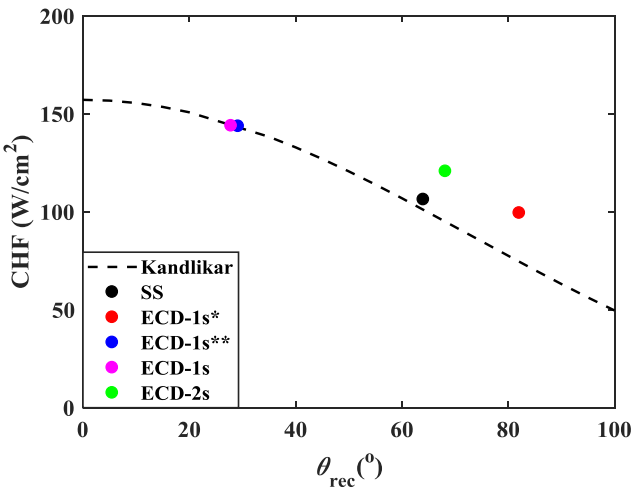

Figure 4.19: CHF comparison between the Kandlikar model and experimental values.

Figure 4.19 compares the experimental critical heat fluxes and the predicted values by the Kandlikar model, which indicates that the model can well predict the present results. Therefore, concerning water boiling, it is important to lower the receding contact angles to enhance the critical heat flux.

However, Kandilikar did not consider the effect of surface characteristics, e.g., roughness on the forces, which is probably the reason why the model may underestimate the critical heat flux. Accordingly, the Kandlikar model was further developed, by considering a wicking

force (F_w) and a roughness-factor-dependent surface tension force (F_{s2}) on modified surfaces, as shown in Fig. 4.20.

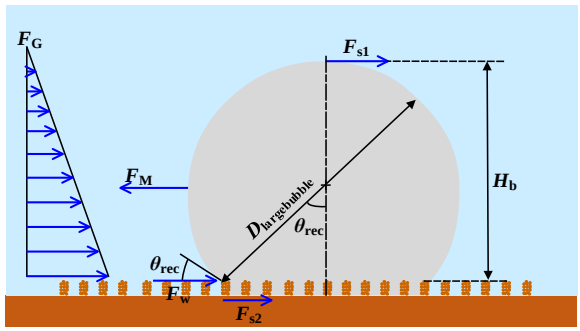

Figure 4.20: Schematics of the modified Kandlikar model.

The detailed derivation process is available in **Paper iv**, and the final expression is as follows

$$\mathrm{CHF} = i_{lv} \cdot \rho_v^{1/2} \cdot [\sigma_{lv} g(\rho_l - \rho_v)]^{1/4} \cdot \left(\frac{1+\cos\theta_{rec}}{16}\right) \cdot \left[\frac{2}{\pi} \cdot r + \frac{\pi}{4}(1+\cos\theta_{rec})\right]^{1/2} \quad (4\text{-}13)$$

where, r is the roughness factor, describing the surface area enhancement ratio.

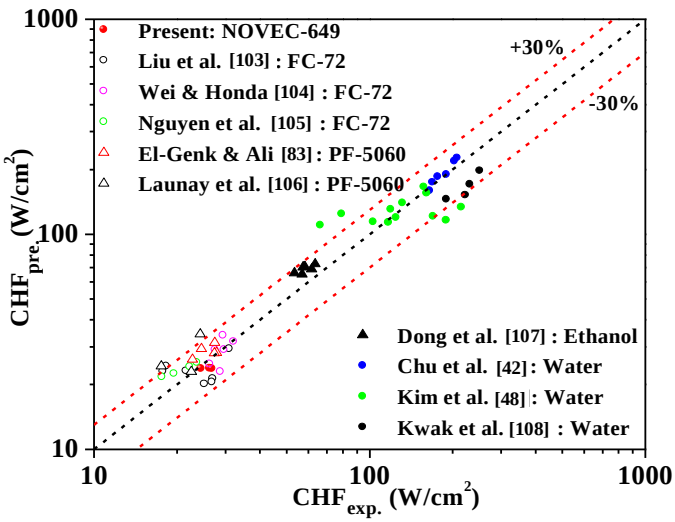

Figure 4.21: CHF comparison between the modified Kandlikar model and experimental values.

To validate the model by Eq. (4-13), the experimental results in **Paper iv** and literature data were compared with the model. Different liquids were compared, i.e., NOVEC-649 in this work, FC-72 in [103-105], PF5060 in [83, 106], ethanol in [107] and water in [42, 48, 108]. Figure 4.21 shows the comparison of the results, which indicates that the present model provides good prediction, with a deviation within ±30% for most of the data points. However,

the deficiencies of the present model are also discussed here. The present model, along with the models by Chu et al. [42] and Quan et al. [43], indicates that CHF increases with increasing roughness factor, for well-wetting liquids with relatively low contact angle. However, this is not totally consistent with some results in literature, e.g., [103, 104]. In addition, it is tricky to calculate or estimate the roughness factor on some modified surfaces which have quite irregular and non-uniform structures.

In summary, possible critical heat flux mechanisms were analyzed in this section. The wickability, which characterizes the ability of liquid supplement, is considered as an important parameter that determines the critical heat flux. A correlation, considering the wickability effect, shows good predictions for the well-wetting liquids. In addition, the receding contact angle is another essential parameter, especially for water. Accordingly, the Kandilikar model was further developed by considering a wicking force (F_w) and a roughness-factor-dependent surface tension force (F_{s2}). Relatively good predictions were achieved.

CHAPTER 5

Conclusions and Outlook

This thesis aims to enhance boiling performance by surface modifications. Several methods were attempted to modify surfaces, including the electrophoretic deposition method, the electrochemical deposition method, the electrostatic deposition methods and the femtosecond laser technique. With these methods, nanoparticle-coating surfaces, microporous surfaces and hybrid micro/nano-structure surfaces were prepared. Following, pool boiling of well-wetting liquids, i.e., dielectric liquids (HFE-7200, NOVEC-649 and FC-72) and organic liquids (Acetone and Pentane), and DI water were comparatively studied on these structured surfaces and smooth surfaces. Then, bubble dynamics, i.e., single bubble nucleation, bubble departure diameter and bubble departure frequency, were experimentally investigated. Accordingly, heat transfer mechanisms and critical heat flux mechanisms were analyzed. At the end, mechanistic heat transfer models were constructed to predict the heat transfer performance, and critical heat flux models were further developed based on existing ones.

5.1 Conclusions

- Regarding pool boiling of well-wetting liquids on nanoparticle-coating surfaces, heat transfer coefficients are significantly enhanced. For example, a maximum 100% enhancement is achieved for HFE-7200. However, the homogeneous nanoparticle coatings cannot enhance the critical heat flux of well-wetting liquids, e.g., HFE-7200, Acetone and Pentane, while the further developed heterogeneous nanoparticle coatings can enhance the critical heat flux, due to the tailored hydrodynamics instability wavelength.
- Regarding pool boiling of well-wetting liquids and DI water on microporous surfaces, heat transfer coefficients and the critical heat flux are both enhanced. For example, maximum 600% and 55% enhancements are obtained for NOVEC-649, concerning the heat transfer coefficient and the critical heat flux, respectively, while maximum 56% and 35% enhancements are obtained for water, concerning the heat transfer coefficient and the critical heat flux, respectively.

- Regarding pool boiling of well-wetting liquids on the hybrid micro/nano-structure surfaces, in general, the heat transfer coefficient and the critical heat flux can be further enhanced by the hybrid micro/nano structures, For example, heat transfer coefficients on surfaces combining micro pin fins with nanoparticle coatings are further enhanced by 15% - 33%, in comparison to the micro-pin-fin surfaces, though the critical heat flux changes slightly.
- The coating surfaces, including the nanoparticle coatings and microporous coatings, have a smaller bubble departure diameter and a higher bubble departure frequency, in comparison to smooth surfaces. It is also found that more bubbles nucleate on the coating surfaces, than on smooth surfaces. These are contributing to the heat transfer enhancement.
- Mechanistic heat transfer models, involving the natural convection, the transient conduction, the transient micro convection and the microlayer evaporation show good prediction of the heat transfer performance, but the transient conduction and the transient micro convection contribute the most.
- Surface wickability is quantitatively compared. Results indicate that for well-wetting liquids, the critical heat flux depends on the wickability. For example, the critical heat flux of HFE-7200 is not enhanced on the homogeneous nanoparticle-particle surfaces on which the wickability is not enhanced. However, for water, it is found that the critical heat flux is enhanced on the hydrophobic surfaces with low receding contact angles, but not enhanced on the hydrophobic surfaces with high receding contact angles. Accordingly, the Kandlikar model, involving the receding contact angle, well predicts the corresponding results. At the end, the Kandlikar model is further developed, considering the effect of surface characteristics on forces, showing good predictions for both well-wetting liquids and water.

5.2 Outlook

Boiling heat transfer has been investigated extensively for several decades. However, it is still far away from the “truth” in boiling and surface durability is also a big issue in practice. Accordingly, some possible future works are discussed as follows

- From the perspective of mechanistic studies, advanced techniques are recommended to understand bubble nucleation and interaction (related to heat transfer), and critical heat flux, such as advanced imaging techniques, e.g., tomography techniques, PIV techniques and infrared visualizations. In addition, numerical simulations are also recommended to assist in understanding the mechanism.
- Even though, numerous enhanced surfaces have been reported, it is relatively rare about the single effect of surface characteristics, e.g., surface roughness and surface wettability. To study the single effect is helpful to understand relevant mechanisms.
- From the perspective of practical application, surface durability needs to be further considered. In addition, flow boiling, which is more common in practice, needs to be investigated in the next step.

Summary of Papers

Paper i: Pool boiling of HFE-7200 on nanoparticle-coating surfaces: Experiments and heat transfer analysis

***Zhen Cao**, Zan Wu, AnhDuc Pham, Yanjie Yang, Sahar Abbood, Peter Falkman, Tautgirdas Ruzgas, Cathrine Albèr, Bengt Sundén*

International Journal of Heat and Mass Transfer, 2019, Vol. 133, pp. 548-560

In this paper, pool boiling of HFE-7200 was experimentally studied on homogeneous nanoparticle-coating surfaces. In comparison to the smooth surface, the heat transfer coefficient was considerably enhanced, while the critical heat flux was not augmented. A mechanistic heat transfer model was developed, considering natural convection, transient heat conduction and microlayer evaporation. The model showed a good prediction, especially at low heat fluxes.

I did the experiments, analyzed the data and wrote the paper. AnhDuc Pham prepared the surfaces. Bengt Sundén and Zan Wu helped with technical suggestions, gave feedback and proofread the paper.

Paper ii: Electrophoretic deposition surfaces to enhance HFE-7200 pool boiling heat transfer and critical heat flux

***Zhen Cao**, Zan Wu, Anh-Duc Pham, Bent Sundén*

International Journal of Thermal Sciences, 2019, Vol. 146, pp. 106107

This paper is a continuation of the studies in Paper i. Heterogeneous nanoparticle-coating surfaces were studied in this paper, instead of homogeneous nanoparticle-coating surfaces. Both the heat transfer coefficient and the critical heat flux were enhanced. The heat transfer was analyzed with the mechanistic model in Paper i, while the critical heat flux was analyzed with the hydrodynamic instability model.

I did the experiments, analyzed the data and wrote the paper. AnhDuc Pham prepared the surfaces. Bengt Sundén and Zan Wu helped with technical suggestions, gave feedback and proofread the paper.

Paper iii: Saturated pool boiling heat transfer of acetone and HFE-7200 on modified surfaces by electrophoretic and electrochemical deposition

*Zan Wu, **Zhen Cao**, Bengt Sundén*

Applied Energy, 2019, Vol. 249, pp. 286-299

This paper is a continuation of the studies in Paper i and Paper ii. Except the nanoparticle-coating surfaces, microporous-coating surfaces were prepared by an electrochemical deposition method, and pool boiling of acetone was investigated as well. It was seen that the

nanoparticle-coating surfaces still only enhanced the heat transfer coefficient, but the microporous-coating surfaces enhanced both the heat transfer coefficient and the critical heat flux. Another mechanistic heat transfer model was developed, involving transient heat conduction, transient micro convection and microlayer evaporation, which also shows a good prediction.

The experiments were performed together with Zan Wu. Zan Wu analyzed the data and wrote the paper. Bengt Sundén and I gave feedback and proofread the paper.

Paper iv: Heat transfer prediction and critical heat flux mechanism for pool boiling of NOVEC-649 on microporous copper surfaces
***Zhen Cao**, Zan Wu, Bengt Sundén*
International Journal of Heat and Mass Transfer, 2019, Vol. 141, pp. 818-834

This paper is a continuation of the studies in Paper iii, while this paper focused on empirical prediction of the heat transfer coefficient and mechanisms of the critical heat flux, regarding pool boiling of NOVEC-649 on microporous-coating surfaces. The Rohsenow correlation was modified, and the Kandlikar model was further developed.

I did the experiments, analyzed the data and wrote the paper. Bengt Sundén and Zan Wu helped with technical suggestions, gave feedback and proofread the paper.

Paper v: Pool boiling of water on coating surfaces: bubble dynamics, heat transfer and critical heat flux
***Zhen Cao**, Zan Wu, Bengt Sundén*
Submitted for Journal publication (under review)

This paper is a continuation of the studies in Paper iv. Pool boiling of water on microporous-coating surfaces was investigated, concerning bubble nucleation, heat transfer and critical heat flux. Especially, the process of bubble evolution was captured, and bubble departure diameters and frequencies were quantitatively studied.

I did the experiments, analyzed the data and wrote the paper. Bengt Sundén and Zan Wu helped with technical suggestions, gave feedback and proofread the paper.

Paper vi: Pool boiling heat transfer of N-pentane on micro/nanostructured surfaces
*Bin Liu, **Zhen Cao**, Yonghai Zhang, Zan Wu, AnhDuc Pham, Wenjun Wang, Zhaoxuan Yan, Jinjia Wei, Bengt Sundén*
International Journal of Thermal Sciences, 2018, Vol. 130, pp. 386-394

This paper focused on pool boiling of pentane on micro/nano-structured surfaces. The hybrid micro/nano-structured surfaces exhibited the best pool boiling performance, concerning the

heat transfer coefficient and the critical heat flux. The wickability enhancement was attributed to the critical heat flux mechanism.

I prepared the experimental setup, and the experiments were performed together with Bin Liu. Bin Liu analyzed the data and wrote the paper. Bengt Sundén, Jinjia Wei, Zan Wu and Yonghai Zhang helped with technical suggestions, gave feedback and proofread the paper.

Paper vii: Pool boiling heat transfer of FC-72 on pin-fin silicon surfaces with nanoparticle deposition

***Zhen Cao**, Bin Liu, Calle Preger, Zan Wu, Yonghai Zhang, Xueli Wang, Maria E. Messing, Knut Deppert, Jinjia Wei, Bengt Sundén*

International Journal of Heat and Mass Transfer, 2018, Vol. 126, pp. 1019-1033

This paper studied subcooled pool boiling of FC-72 on silicon surfaces with micro pin fins and hybrid micro/nano structures. Both the heat transfer coefficient and the critical heat flux were considerably enhanced, and a correlation, concerning subcooling and wickability, was proposed to predict the current critical heat fluxes.

Bin Liu and Calle Preger prepared the surfaces, and the experiments were performed together with Bin Liu. I analyzed the data and wrote the paper. Bengt Sundén, Jinjia Wei, Zan Wu and Yonghai Zhang helped with technical suggestions, gave feedback and proofread the paper.

References

[1] M. Hohr, Technology leadership. *Technology and Manufacturing Day*, 2017.
[2] E. Mudawar, Assessment of high-heat-flux thermal management schemes, *IEEE Transactions on Componenets and Packaging Technologies*, 24 (2001) 122-141.
[3] Datacom equipment power trends and cooling applications, 2nd Edition. American Society of Heating Refrigerating and Air-Conditioning Engineers 2012.
[4] http://energy.mit.edu/news/bubble-bubble-boiling-on-the-double/.
[5] S. Nukiyama, The maximum and minimum values of the heat *Q* transmitted from metal to boiling water under atmopheric pressure, *Internatinal Journal of Heat Mass Transfer* 9 (1966) 1419-1433.
[6] R. Cole, Boiling nucleation, *Advances in Heat Transfer* 10 (1974) 85-166.
[7] D. Wu, Y.Y. Duan, Z. Yang, Themodynamic model for heterogeneous bubble nucleation in a temperature gradient, *Applied Physics Letters*, 97 (2010) 081911.
[8] X. Quan, G. Chen, P. Cheng, A thermodynamic analysis for heterogeneous boiling nucleation on a superheated wall, *International Journal of Heat and Mass Transfer*, 54 (2011) 4762-4769.
[9] C. Courty, Surface variables in nucleate boiling, Ph.D Thesis, Purdue Univiversity, 1952.
[10] P. Griffith, D. Wallis, The Role of Surface Conditions in Nucleate Boiling, *Technical Report* 14 (1958), Massachusetts Institute of Technology.
[11] S.G. Bankoff, Entrapment of gas in the spreading of a liquid over a rough surface, *AIChE Journal*, 4 (1958) 24-26.
[12] H.H. Hsu, On the size range of active nucleation cavities on a heating surface, *Journal of Heat Transfer*, 84 (1962) 207-213.
[13] C.Y. Han, P. Griffith, The mechanism of heat transfer in nucleate pool boiling-part I bubble initiation, growth and departure, *International Journal of Heat Mass Transfer*, 8 (1965) 887-904.
[14] H.K. Forster, N. Zuber, Dynamics of vapor bubbles and boiling heat transfer, *AIChE Journal*, 1 (1955) 531-535.
[15] W.M. Rohsenow, A method of correlating heat transfer data for surface boiling of liquids, *Technical Reptort* 5 (1951), Massachusetts Institute of Technology.
[16] C.L. Tien, A hydrodynamic model for nucleate pool boiling, *International Journal of Heat and Mass Transfer*, 5 (1962) 533-540.
[17] C.Y. Han, P. Griffith, The mechanism of heat transfer in nucleate pool boiling-Part II, *International Journal of Heat and Mass Transfer*, 8 (1965) 905-914.
[18] B.B. Mikic, W.M. Rohsenow, A new correlation of pool boiling data including the effect of heating surface characteristics, *Journal of Heat Transfer*, 91 (1969) 245-250.
[19] R.J. Benjamin, A.R. Balakrishnan, Nucleate pool boiling heat transfer of pure liquids at low to moderate heat fluxes, *International Journal of Heat and Mass Transfer*, 39 (1996) 2495-2504.
[20] Z. Guo, M. El-Genk, Liquid microlayer evaporatin during nucleate boiling on the surface of a flat composite wall, *International Journal of Heat and Mass Transfer*, 37 (1994) 1641-1655.

[21] V. Sernas, F.C. Hooper, The initial vapor bubble growth on a heated wall during nucleate boiling, *International Journal of Heat abd Mass Transfer*, 12 (1969) 1627-1639.
[22] M.G. Cooper, A.J.P. Lloyd, The microlayer in nucleate pool boiling, *International Journal of Heat and Mass Transfer*, 12 (1969) 895-913.
[23] C.M. Voutsinos, R.L. Judd, Laser interferometric investigation of the microlayer evaporation phenomenon, *Journal of Heat Transfer*, 97 (1975) 88-92.
[24] Y.Y. Li, Z.H. Liu, G.S. Wang, A predictive model of nucleate pool boiling on heated hydrophilic surfaces, *International Journal of Heat and Mass Transfer*, 65 (2013) 789-797.
[25] S.I. Haider, R.L. Webber, The microlayer in nucleate pool boiling, *International Journal of Heat and Mass Transfer*, 40 (1997) 3675-3688.
[26] K. Stephan, M. Abdelsalam, Heat-transfer correlations for natural convection boiling, *International Journal of Heat and Mass Transfer*, 23 (1980) 73-87.
[27] K. Nishikawa, Y. Fujita, H. Ohta, S. Hidaka, Effects of system pressure and surface roughness on nucleate boiling heat transfer, Memoirs of the Faculty of Engineering, Kyushu Univeristy, 42 (1982) 95-111.
[28] M.G. Cooper, Heat flow rates in saturated nucleate pool boiling-a wide-ranging examination using reduced properties, *Advances in Heat Transfer*, 16 (1984) 157-239.
[29] D. Gorenflo, D. Kenning, "Pool boiling" VDI Heat Atlas, VDI-Verlag GmbH, Dusseldorf 2010.
[30] W. Leiner, Heat transfer by nucleate pool boiling-general correlation based on thermodynamic similarity, *International Journal of Heat and Mass Transfer*, 37 (1994) 763-769.
[31] G. Ribatski, J.M.S. Jabardo, Experimental study of nucleate boiling of halocarbon refrigerants on cylindrical surfaces, *International Journal of Heat and Mass Transfer*, 46 (2003) 4439-4451.
[32] J. Kim, Review of nucleate pool boiling bubble heat transfer mechanisms, *International Journal of Multiphase Flow*, 35 (2009) 1067-1076.
[33] R.L. Mohanty, M.K. Das, A critical review on bubble dynamics parameters influencing boiling heat transfer, *Renewable and Sustainable Energy Reviews*, 78 (2017) 466-494.
[34] N. Zuber, Hydrodynamic aspects of boiling heat transfer, PhD Thesis, University of California, 1959.
[35] Y. Haramura, Y. Katto, A new hydrodynamic model of critical heat flux, applicable widely to both pool and forced convection boiling on submerged bodies in saturated liquids, *International Journal of Heat and Mass Transfer*, 26 (1983) 389-399.
[36] V.V. Yagov Is a crisis in pool boiling actually a hydrodynamic phenomenon?, *International Journal of Heat and Mass Transfer*, 73 (2014) 265-273.
[37] I.C. Chu, H.C. No, C.H. Song, Visualization of boiling structure and critical heat flux phenomenon for a narrow heating surface in a horizontal pool of saturated water, *International Journal of Heat and Mass Transfer*, 62 (2013) 142-152.
[38] H. Zhao, A. Williams, Predicting the critical heat flux in pool boiling based on hydrodynamic instability induced irreversible hot spots, *International Journal of Multiphase Flow*, 104 (2018) 174-184.
[39] C.K. Guan, J.F. Klausner, R. Mei, A new mechanistic model for pool boiling CHF on horizontal surfaces, *International Journal of Heat and Mass Transfer*, 54 (2011) 3960-3969.
[40] S.G. Kandlikar, A theoretical model to predict pool boiling CHF incorporating effects of contact angle and orientation, *Journal of Heat Transfer*, 123 (2001) 1071-1079.

[41] M.M. Rahman, E. Olceroglu, M. McCarthy, Role of wickability on the critical heat flux of structured superhydrophilic surfaces, Langmuir, 30 (2014) 11225-11234.
[42] K.H. Chu, R. Enright, E.N. Wang, Structured surfaces for enhanced pool boiling heat transfer, *Applied Physics Letters*, 100 (2012) 241603.
[43] X. Quan, L. Dong, P. Cheng, A CHF model for saturated pool boiling on a heated surface with micro/nano-scale structures, *International Journal of Heat and Mass Transfer*, 76 (2014) 452-458.
[44] W. Ding, E. Krepper, U. Hampel, Quantitative prediction of critical heat flux initiation in pool and flow boiling, *International Journal of Thermal Sciences*, 125 (2018) 121-131.
[45] G. Liang, I. Mudawar, Pool boiling critical heat flux (CHF) – Part 1: Review of mechanisms, models, and correlations, *International Journal of Heat and Mass Transfer*, 117 (2018) 1352-1367.
[46] D. Lee, N. Lee, D.I. Shim, B.S. Kim, H.H. Cho, Enhancing thermal stability and uniformity in boiling heat transfer using micro-nano hybrid surfaces (MNHS), *Applied Thermal Engineering*, 130 (2018) 710-721.
[47] H.W. Moon, Y.J. Yoon, J.H. Park, B.S. Myung, D.E. Kim, Dynamic wetting and boiling characteristics on micro-structured and micro/nano hierarchically structured surfaces, *Experimental Thermal and Fluid Science*, 74 (2016) 19-26.
[48] S.H. Kim, G.C. Lee, J.Y. Kang, K. Moriyama, M.H. Kim, H.S. Park, Boiling heat transfer and critical heat flux evaluation of the pool boiling on micro structured surface, *International Journal of Heat and Mass Transfer*, 91 (2015) 1140-1147.
[49] N.S. Dhillon, J. Buongiorno, K.K. Varanasi, Critical heat flux maxima during boiling crisis on textured surfaces, *Nature Communications*, 6 (2015) 8247.
[50] B.S. Kim, H. Lee, S. Shin, G. Choi, H.H. Cho, Interfacial wicking dynamics and its impact on critical heat flux of boiling heat transfer, *Applied Physics Letters*, 105 (2014) 191601.
[51] J.J. Wei, L.J. Guo, H. Honda, Experimental study of boiling phenomena and heat transfer performances of FC-72 over micro-pin-finned silicon chips, *Heat and Mass Transfer*, 41 (2005) 744-755.
[52] C. Li, G.P. Peterson, Evaporation/Boiling in Thin Capillary Wicks (II)—Effects of Volumetric Porosity and Mesh Size, *Journal of Heat Transfer*, 128 (2006) 1320.
[53] D.H. Min, G.S. Hwang, Y. Usta, O.N. Cora, M. Koc, M. Kaviany, 2-D and 3-D modulated porous coatings for enhanced pool boiling, *International Journal of Heat and Mass Transfer*, 52 (2009) 2607-2613.
[54] Ö.N. Cora, D. Min, M. Koç, M. Kaviany, Microscale-modulated porous coatings: fabrication and pool-boiling heat transfer performance, J*ournal of Micromechanics and Microengineering*, 20 (2010) 035020.
[55] X.B. Ji, J.L. Xu, Z.W. Zhao, W.L. Yang, Pool boiling heat transfer on uniform and non-uniform porous coating surfaces, *Experimental Thermal and Fluid Science*, 48 (2013) 198-212.
[56] R. Pastuszko, T.M. Wójcik, Experimental investigations and a simplified model for pool boiling on micro-fins with sintered perforated foil, *Experimental Thermal and Fluid Science*, 63 (2015) 34-44.
[57] A.K. Das, P.K. Das, P. Saha, Performance of different structured surfaces in nucleate pool boiling, *Applied Thermal Engineering*, 29 (2009) 3643-3653.

[58] A.M. Gheitaghy, H. Saffari, M. Mohebbi, Investigation pool boiling heat transfer in U-shaped mesochannel with electrodeposited porous coating, *Experimental Thermal and Fluid Science*, 76 (2016) 87-97.
[59] Y. Tang, J. Zeng, S. Zhang, C. Chen, J. Chen, Effect of structural parameters on pool boiling heat transfer for porous interconnected microchannel nets, *International Journal of Heat and Mass Transfer*, 93 (2016) 906-917.
[60] E. Akbari, A.M. Gheitaghy, H. Saffari, S.M. Hosseinalipour, Effect of silver nanoparticle deposition in re-entrant inclined minichannel on bubble dynamics for pool boiling enhancement, *Experimental Thermal and Fluid Science*, 82 (2017) 390-401.
[61] Y. Sun, G. Chen, S. Zhang, Y. Tang, J. Zeng, W. Yuan, Pool boiling performance and bubble dynamics on microgrooved surfaces with reentrant cavities, *Applied Thermal Engineering*, 125 (2017) 432-442.
[62] C.M. Kruse, T. Anderson, C. Wilson, C. Zuhlke, D. Alexander, G. Gogos, S. Ndao, Enhanced pool-boiling heat transfer and critical heat flux on femtosecond laser processed stainless steel surfaces, *International Journal of Heat and Mass Transfer*, 82 (2015) 109-116.
[63] J.Y. Ho, K.K. Wong, K.C. Leong, Saturated pool boiling of FC-72 from enhanced surfaces produced by Selective Laser Melting, *International Journal of Heat and Mass Transfer*, 99 (2016) 107-121.
[64] K.K. Wong, K.C. Leong, Saturated pool boiling enhancement using porous lattice structures produced by Selective Laser Melting, *International Journal of Heat and Mass Transfer*, 121 (2018) 46-63.
[65] B. Liu, J. Liu, J. Zhou, B. Yuan, Y. Zhang, J. Wei, W. Wang, Experimental study of subcooled boiling pool heat transfer and its "hook back" phenomenon on micro/nanostructured surfaces, *International Communications in Heat and Mass Transfer*, 100 (2019) 73-82.
[66] C. Zhang, L. Zhang, H. Xu, P. Li, B. Qian, Performance of pool boiling with 3D grid structure manufactured by selective laser melting technique, *International Journal of Heat and Mass Transfer*, 128 (2019) 570-580.
[67] S.B. White, A.J. Shih, K.P. Pipe, Boiling surface enhancement by electrophoretic deposition of particles from a nanofluid, *International Journal of Heat and Mass Transfer*. 54 (2011) 4370-4375.
[68] S. Jun, S. Sinha-Ray, A.L. Yarin, Pool boiling on nano-textured surfaces, *International Journal of Heat and Mass Transfer*, 62 (2013) 99-111.
[69] R.P. Sahu, S. Sinha-Ray, S. Sinha-Ray, A.L. Yarin, Pool boiling on nano-textured surfaces comprised of electrically-assisted supersonically solution-blown, copper-plated nanofibers: Experiments and theory, *International Journal of Heat and Mass Transfer*, 87 (2015) 521-535.
[70] K.C. Pratik, A. Nammari, T.S. Ashton, A.L. Moore, Saturated pool boiling heat transfer from vertically oriented silicon surfaces modified with foam-like hexagonal boron nitride nanomaterials, *International Journal of Heat and Mass Transfer*, 95 (2016) 964-971.
[71] S. Das, B. Saha, S. Bhaumik, Experimental study of nucleate pool boiling heat transfer of water by surface functionalization with SiO2 nanostructure, *Experimental Thermal and Fluid Science*, 81 (2017) 454-465.
[72] S. Das, B Saha, S. Bhaumik, Experimental study of nucleate pool boiling heat transfer of water by surface functionalization with crystalline TiO2 nanostructure, *Applied Thermal Engineering*, 113 (2017) 1345-1357.

[73] H.S. Jo, S. An, H.G. Park, M.W. Kim, S.S. Al-Deyab, S.C. James, J. Choi, S.S. Yoon, Enhancement of critical heat flux and superheat through controlled wettability of cuprous-oxide fractal-like nanotextured surfaces in pool boiling, *International Journal of Heat and Mass Transfer*, 107 (2017) 105-111.
[74] A.M. Gheitaghy, H. Saffari, D. Ghasimi, A. Ghasemi, Effect of electrolyte temperature on porous electrodeposited copper for pool boiling enhancement, *Applied Thermal Engineering*, 113 (2017) 1097-1106.
[75] Y.Q. Wang, J.L. Luo, Y. Heng, D.C. Mo, S.S. Lyu, Wettability modification to further enhance the pool boiling performance of the micro nano bi-porous copper surface structure, *International Journal of Heat and Mass Transfer*, 119 (2018) 333-342.
[76] A.M. Rishi, A. Gupta, S.G. Kandlikar, Improving aging performance of electrodeposited copper coatings during pool boiling, *Applied Thermal Engineering*, 140 (2018) 406-414.
[77] H.H. Son, S.J. Kim, Role of receding capillary flow correlating nano/micro scale surface roughness and wettability with pool boiling critical heat flux, *International Journal of Heat and Mass Transfer*, 138 (2019) 985-1001.
[78] G. Liang, I. Mudawar, Review of pool boiling enhancement by surface modification, *International Journal of Heat and Mass Transfer*, 128 (2019) 892-933.
[79] D.E. Kim, D.I. Yu, D.W. Jerng, M.H. Kim, H.S. Ahn, Review of boiling heat transfer enhancement on micro/nanostructured surfaces, *Experimental Thermal and Fluid Science*, 66 (2015) 173-196.
[80] C.M. Patil, S.G. Kandlikar, Review of the Manufacturing Techniques for Porous Surfaces Used in Enhanced Pool Boiling, *Heat Transfer Engineering*, 35 (2013) 887-902.
[81] R.J. Moffat, Describing the uncertainties in experimental results, *Experimental Thermal and Fluid Science*, 1 (1988) 3-17.
[82] R.I. Vachon, G.H. Nix, G.E. Tanger, Evaluation of constants for the Rohsenow pool-boiling correlation, *Journal of Heat Transfer*, 90 (1968) 239-246.
[83] M.S. El-Genk, A.F. Ali, Enhanced nucleate boiling on copper micro-porous surfaces, *International Journal of Multiphase Flow*, 36 (2010) 780-792.
[84] S. Siedel, S. Cioulachtjian, J. Bonjour, Experimental analysis of bubble growth, departure and interactions during pool boiling on artificial nucleation sites, *Experimental Thermal and Fluid Science*, 32 (2008) 1504-1511.
[85] Y. Nam, J. Wu, G. Warrier, Y.S. Ju, Experimental and numerical study of single bubble dynamics on a hydrophobic surface, *Journal of Heat Transfer*, 131 (2009) 121004.
[86] H. Jo, H.S. Ahn, S. Kang, M.H. Kim, A study of nucleate boiling heat transfer on hydrophilic, hydrophobic and heterogeneous wetting surfaces, *International Journal of Heat and Mass Transfer*, 54 (2011) 5643-5652.
[87] B. Shen, M. Yamada, S. Hidaka, J. Liu, J. Shiomi, G. Amberg, M. Do-Quang, M. Kohno, K. Takahashi, Y. Takata, Early Onset of Nucleate Boiling on Gas-covered Biphilic Surfaces, *Scientific Reports*, 7 (2017) 2036.
[88] T.P. Allred, J.A. Weibel, S.V. Garimella, The petal effect of parahydrophobic surfaces offers low receding contact angles that promote effective boiling, *International Journal of Heat and Mass Transfer*, 135 (2019) 403-412.
[89] M. Jakob, Heat Transfer, New York: Wiley and Sons, 1949.
[90] P.W. Mcfadden, P. Grassmann, The relation between bubble frequency and diameter during nucleate pool boiling, *International Journal of Heat and Mass Transfer*, 5 (1962) 169-173.

[91] N. Zuber, Nucleate boiling. the region of isolated bubbles and the similarity with natural convection, *International Journal of Heat and Mass Transfer*, 6 (1963) 53-78.
[92] R. Cole, Bubble frequencies and departure volumes at subatmopheric pressures, *AIChE Journal*, 13 (1967) 779-783.
[93] H.J. Ivey, Relationships between bubble frequency, departure diameter and rise velocity in nucleate boiling, *International Journal of Heat and Mass Transfer*, 10 (1967) 1023-1040.
[94] J.G. Collier, J.R. Thome, Convective Boiling and Condensation, Oxford University Press, 1994.
[95] H.T. Phan, N. Caney, P. Marty, S. Colasson, J. Gavillet, How does surface wettability influence nucleate boiling?, *Comptes Rendus Mécanique*, 337 (2009) 251-259.
[96] J. Kim, B.D. Oh, M.H. Kim, Experimental study of pool temperature effects on nucleate pool boiling, *International Journal of Multiphase Flow*, 32 (2006) 208-231.
[97] G. Kocamustafaogullari, M. Ishii, Interfacial area and nucleation site density in boiling systems, *International Journal of Heat and Mass Transfer*, 26 (1983) 1377-1387.
[98] C.H. Wang, V.K. Dhir, Effect of surface wettability on active nucleation site density during pool boiling of water on a vertical surface, *Journal of Heat Transfer*, 115 (1993) 659-669.
[99] N. Basu, G.R. Warrier, V.K. Dhir, Onset of nucleate boiling and active nucleation site density during subcooled flow boiling, *Journal of Heat Transfer*, 124 (2002) 717.
[100] T. Hibiki, M. Ishii, Active nucleation site density in boiling systems, *International Journal of Heat and Mass Transfer*, 46 (2003) 2587-2601.
[101] S.J. Thiagarajan, R. Yang, C. King, S. Narumanchi, Bubble dynamics and nucleate pool boiling heat transfer on microporous copper surfaces, *International Journal of Heat and Mass Transfer*, 89 (2015) 1297-1315.
[102] H.S. Ahn, H.J. Jo, S.H. Kang, M.H. Kim, Effect of liquid spreading due to nano/microstructures on the critical heat flux during pool boiling, *Applied Physics Letters*, 98 (2011) 071908.
[103] B. Liu, J. Liu, Y. Zhang, J. Wei, W. Wang, Experimental and theoretical study of pool boiling heat transfer and its CHF mechanism on femtosecond laser processed surfaces, *International Journal of Heat and Mass Transfer*, 132 (2019) 259-270.
[104] J.J. Wei, H. Honda, Effects of fin geometry on boiling heat transfer from silicon chips with micro-pin-fins immersed in FC-72, *International Journal of Heat and Mass Transfer*, 46 (2003) 4059-4070.
[105] T.B. Nguyen, D. Liu, M.I. Kayes, B. Wang, N. Rashin, P.W. Leu, T. Tran, Critical heat flux enhancement in pool boiling through increased rewetting on nanopillar array surfaces, *Scientific Reports*, 8 (2018) 4815.
[106] S. Launay, A.G. Fedorov, Y. Joshi, A. Cao, P.M. Ajayan, Hybrid micro-nano structured thermal interfaces for pool boiling heat transfer enhancement, *Microelectronics Journal*, 37 (2006) 1158-1164.
[107] L. Dong, X. Quan, P. Cheng, An experimental investigation of enhanced pool boiling heat transfer from surfaces with micro/nano-structures, *International Journal of Heat and Mass Transfer*, 71 (2014) 189-196.
[108] H.J. Kwak, J.H. Kim, B.S. Myung, M.H. Kim, D.E. Kim, Behavior of pool boiling heat transfer and critical heat flux on high aspect-ratio microchannels, *International Journal of Thermal Sciences*, 125 (2018) 111-120.